Nanostructured metal oxide doped hydrogel based biosensor for biomedical application

A major project dissertation submitted in partial fulfillment of the requirement

for the degree

of

Master of Technology

In

Industrial Biotechnology

Submitted by

SHWETA PANWAR

Regn. No.: DTU/14/M.TECH/097

Under the supervision of

Prof. Bansi. D. Malhotra

Department of Biotechnology,
Delhi Technological University,
Delhi-110042, India

DECLARATION

I, **Shweta Panwar,** hereby declare that the M. Tech. dissertation entitled **"Nanostructured metal oxide doped hydrogel based biosensor for biomedical application"** submitted in partial fulfillment of the requirement for the award of the degree of Master of Technology (Industrial Biotechnology), Delhi Technological University, is a record of original and independent research work done by me under the supervision and guidance of **Prof. Bansi. D. Malhotra**, Department of Biotechnology, Delhi Technological University, Delhi. The information and data enclosed in the dissertation is original and has not formed the basis of the award of any degree/ diploma/fellowship or other similar title to any candidate of the university/institution.

Date:

(Shweta Panwar)
Regn.No. DTU/14/M.TECH/097
M.Tech. (Industrial Biotechnology)
Department of Biotechnology,
Delhi Technological University,
Shahbad Daulatpur,
Main Bawana Road,
Delhi 110042,India

CERTIFICATE

This is to certify that this major report entitled "**Nanostructured metal oxide doped hydrogel based biosensor for biomedical application"** submitted by **Ms. Shweta Panwar (Regn. No.: DTU/14/M.TECH/097)** in the partial fulfilment of the requirements for the reward of the degree of Master of Technology (Industrial Biotechnology), Delhi Technological University, Delhi-110042 is an authentic record of the candidate's own work carried out by her under my guidance. The information and data enclosed in this synopsis is original and has not been submitted elsewhere for honoring of any other degree.

Prof. D. Kumar
Head
Department of Biotechnology
Delhi Technological University
Delhi 110042, India

Prof. Bansi D. Malhotra
Project Mentor
Department of Biotechnology
Delhi Technological University
Delhi-110042, India

ACKNOWLEDGEMENT

By the grace of almighty, I express my profound sense of reverence of gratitude to my mentor Prof. Bansi. D. Malhotra, Department of Biotechnology, Delhi Technological University, Delhi-110042 for his valuable guidance, congenial discussion, incessant help, calm, endurance, constructive criticism and constant encouragement throughout this investigation right from the imitation of work to the shaping of manuscript. I also extend my gratitude to Prof. D. Kumar, Head of the Department of Biotechnology, Delhi Technological University.

I am thankful to and fortunate enough to get constant support and guidance to all the faculty members of the Department of Biotechnology.

I am highly indebted to Mr. Suveen Kumar, Mr. Saurabh Kumar and Ms. Shine Augustine (Research Scholar) for their guidance and constant supervision as well as for providing necessary information regarding the instruments and experiments and also for their support in completing the report. At last but never the least, words are small trophies to express my deep sense of gratitude and affection to Dr. C. M. Pandey, my labmates and my parents who gave me infinite love to go for this achievement. I am also thankful of Mr. C. B. Singh and Mr. Jitender Kumar for successful submission of my thesis.

(SHWETA PANWAR)

2K14/IBT/15

CONTENTS

LIST OF ABBREVIATIONS

Ab	Antibody
APTES	3-Aminopropyl triethoxysilane
AgCl	Silver chloride
SEM	Scanning electron microscopy
BSA	Bovine serum albumin
FTIR	Fourier transform infrared spectroscopy
EDC	N-ethyle-N'-(3-dimethylaminopropyl) carbodiamide
ELISA	Enzyme-linked immunosorbent assay
GG	Guar Gum
GGH/Hydrogel	Guar Gum Hydrogel
JCPDS	Joint Committee on Powder Diffraction Standards
LOD	Limit of detection
NHS	N-hydroxysuccinimide
nMOx	Nanostructured metal oxides
PBS	Phosphate buffer saline
XRD	X-Ray diffraction
CE	Counter electrode
E	Potential
E_{pa}	Anodic peak potential
E_{pc}	Cathodic peak potential
I_{pa}	Anodic peak current
I_{pc}	Cathodic peak current
ng	Nanogram

LIST OF TABLES

LIST OF SCHEMES/FIGURES

CHAPTER 1

ABSTRACT

Nanostructured metal oxide doped hydrogel based biosensor for biomedical application

Shweta Panwar*

***Delhi Technological University, Delhi, India**

firstshweta2014@gmail.com

1. ABSTRACT

This dissertation conatins results of the studies related to the fabrication of nanostructured metal oxide doped guar gum hydrogel (GGH/Hydrogel) based immunosensing platform for detection of oral cancer biomarker (CYFRA-21-1). First of all we have synthesized nanostructured zirconia through hydrothermal process thereafter it has been functionalized with serine amino acid and GGH has been synthesized through chemical process. Further make a mixed solution of nanostructured zirconia with GGH in 1:1 ratio in ddH_2O. The prepared mixture has been further deposited through drop cast method onto pre-hydrolyzed indium oxide (ITO) coated glass electrode. Anti-CYFRA-21-1 has been immobilized through EDC-NHS chemistry and Bovine Serum Albumin (BSA) has been used for blocking of nonspecific binding sites. X-ray diffraction (XRD), scanning electron microscopy (SEM), transmission electron microscopy (TEM), X-ray photoelectron spectroscopy (XPS) and Fourier transform infra-red spectroscopy (FTIR) have been used to investigate the morphological as well as functional characterization of the synthesized material. However, electrochemical studies have been used to characterize fabricated electrodes as well as response studies. The fabricated immunoelectrode (BSA/anti-CYFRA-21-1/Serine/nZrO_2/Hydrogel/ITO) exhibit wider linear detection range (2.5 to 80 ng mL^{-1}), remarkable high sensitivity (0.86 µA mg^{-1} mL cm^{-2}) with shelf life upto 48 days. The electrochemical response studies of fabricated electrode have been further validated through enzyme linked immunosorbent assay (ELISA) on to obtained saliva sample of oral cancer patients.

Keywords: Oral cancer, immunosensor, Guar Gum Hydrogel (GGH/Hydrogel), CYFRA-21-1 and nanostructured zirconium oxide (nZrO_2).

CHAPTER 2

INTRODUCTION

2. INTRODUCTION

Hydrogels have emerged as a potential material in biomaterial field. Smartness, elastomeric nature, softness, porosity, high permeability and capacity to absorb large amount of water makes hydrogel unique biomaterial. The ability of hydrogels to absorb such large amount of water is because of the hydrophilic functional groups attached to the polymer backbone whereas the dissolution arises from the interpenetrating network between polymeric chains.[1] Water inside the hydrogel allows free diffusion of some solute molecules, while the polymeric structure serves as a matrix to hold water together. Likewise, to enhance the electrical conductivity of hydrogel various nanomaterials can be embedded into nanostructured metal oxide, metals, conducting polymers, carbon etc.[2]

Another aspect of the hydrogels is that it is a single polymer molecule because of which the network chains in the gel are connected to each other to form one big molecule on macroscopic scale. That is why it is natural to expect that the conformational changes of the elastically active network chains are visible on the macroscopic level of hydrogel samples. Hydrogel is a state which is neither completely liquid nor completely solid. This state of half liquid-like and half solid-like properties causes many interesting characteristics that are not found in either a pure liquid or solid. While considering its mechanical properties, they are characterized on the basis of elastic modulus which exhibits a pronounced plateau expanding to times at least of the order of seconds, and also on the basis of viscous modulus which is significantly smaller than the elastic modulus in the plateau region.[3] Hydrogels may also demonstrate drastic volume changes in response to external stimuli like solvent and its quality, temperature, electric field and pH. In the last three decades, the change in behaviour of hydrogels received potential interest and work in wider area have been collected in different reviews. Polymeric hydrogel networks can be formed by various methods such as free-radical cross-linking copolymerization and substitution of functional groups via aminating agent or any other reagents.[4-5] The structure of hydrogel and its properties are closely related to the conditions under which it was formed, such as the initial concentration of monomers, cross-linker concentration and the chemistry of the units building the network structure. Therefore, the understanding of the formation mechnisms of hydrogels under different experimental conditions is of great interest to predict their physical properties.[6]

The three-dimensional (3D) structure of hydrogel similar to natural tissues which makes it a promising material in biomaterial application such as biosensor, drug delivery, contact lenses, catheters, wound dressing and tourniquets. This interest has led to their parallel development as the biorecognition layer of potentiometric, conductometric, amperometric and fiber-optic based enzyme biosensors. Because of their high water content, hydrogel membrane layers and gel pads also find application as micro-bioreactors for the hosting and stabilization of biological molecules and for the conduct of biological reactions. Hence, hydrogels have been used to host bioactive layers in several forms of enzyme linked antibody biosensors and DNA biochips. Hydrogel have various applications in the field of biomedical like cancer detection, drug delivery, estimation of metabolites such as glucose, urea, cholesterol, and triglycerides invasively as well non-invasively and fabrication of biosensors etc.[7]

Oral Cancer is the 6^{th} most common cancer and subtype of head and neck cancer. It occurs on the floor of the mouth, lips, cheek lining, gingiva (gums), or palate. The reason behind the oral cancer is mutation, occur at the gene level i.e. APC and p53 due to which uncontrolled cell cycle and differentiation does not take place. Recently, the techniques used for the early detection of oral cancer are laser-capture micro-dissection, visualization adjuncts, cytopathology and biopsy. But these techniques shows several drawbacks such as it require tissue specimen that is highly painful, time consuming, expensive and require skilled personnel for specimen collection.[8] So, there is increasing interest towards non-invasive detection of OC. To overcome the above discussed limitations, biosensor offer a reliable, user-friendly, specific, rapid response time, low cost, sensitive and require low surface volume.

Several amperometric biosensors have been developed for the detection of OC and applied for the non-invasive detection of metabolites in body fluids.[9] Development of miniaturized non-invasive biosensors have been done due to their effective characteristics such as painless, continuous on-line patient monitoring, ready to use analysis report for immediate clinical assistance. Although, non-invasive biosensors are advantageous over the invasive biosensors as they lack properties such as reliability, pain, irritation and chances of infection. Skin, sweat, saliva and urine are used as testing samples for effective diagnosis of oral cancer which are highly convenient to collect and easy to handle for medical professionals.[10]

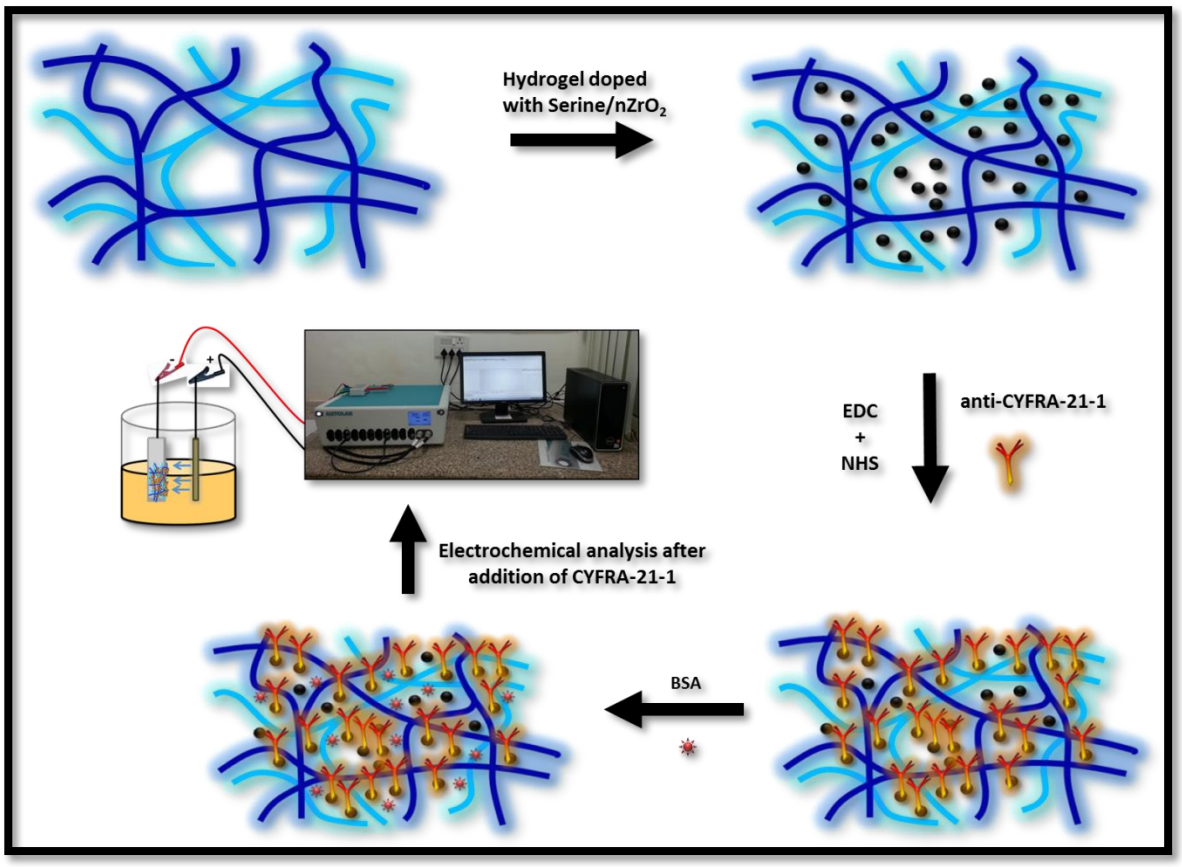

Figure 2.1: Fabrication steps of BSA/anti-CYFRA-21-1/Serine/$nZrO_2$/ITO platform for oral cancer detection.

We have developed a new synthesis method for the preparation of hybrid hydrogels containing functionalized $nZrO_2$ nanoparticles, which were embedded to the polymeric network of natural polysaccharide i.e Guar Gum. In order to incorporate the $nZrO_2$ into the polymer network, the nanoparticles were first functionalized with amine groups by coating them with serine. The presence of amine groups on the surface of the nanoparticles allows immobilization of desired antibody. The novelty of this method consists doping of metal oxide nanoparticles which enhance the electrochemical as well as mechanical properties of Hydrogel. The obtained material is a true hydrogel, capable of swelling in water or physiological solutions. We have used a low temperature hydrothermal method to synthesize nanostructured zirconium oxide ($nZrO_2$) nanoparticles which were incorporated in pre-synthesized hydrogel, synthesized from the natural polysaccharide guar gum. The nanocomposite of hydrogel and serine functionalized nanostructured ZrO_2 has been deposited onto the prehydrolyzed ITO glass electrode via drop cast method and dried at 40℃. Thereafter, the obtained

Serine/nZrO_2/Hydrogel/ITO electrode has been co-immobilized with anti-CYFRA-21-1 antibody and bovine serum albumin (BSA) for CYFRA-21-1 detection. The fabricated immunoelectrode exhibit high sensitivity, low detection range, fast response time and increased shelf life. The results obtained using this electrochemical biosensor have been validated by performing enzyme-linked immunosorbent assay (ELISA).

CHAPTER 3

LITERATURE REVIEW

3.1. Nanostructured metal oxide

Nanomaterials are experiencing a rapid development in recent years due to their potential applications in a wide variety of technological areas such as electronics, catalysis, ceramics, magnetic data storage, structural components, biomaterials, sensors etc. These are defined as materials whose one of the dimensions fall in the size of 1-100 nm, showing peculiar and fascinating chemical, physical and molecular properties along with applications superior than those of their bulk counterparts. Compared to conventional coarse grained counterparts, nanomaterials exhibit increased surface-to-volume ratio, chemical activity, mechanical strength, enhanced diffusivity, higher specific heat and electrical resistivity. Nanomaterials can be classified into nanocrystalline materials and nanoparticles. The former are polycrystalline bulk materials with grain size in the nanometre range (less than 100 nm), while the latter refer to ultrafine dispersive particles with diameters below 100 nm and generally considered as the building blocks of bulk nanocrystalline materials.[11]

The concept of making materials of nanometre size is of fundamental interest. As the size approaches atomic dimensions, energy levels are slowly transferred into quantized discrete energy levels. Further, the reduction in size results in confined electronic motion that affects the physical and chemical properties of materials. Due to the quantum confinement, semiconductor nanoparticles exhibit significant change in their optical and electrical properties. In novel materials, coherent collective oscillations of electrons in the conduction band induce large surface electric field that greatly enhances the radiative properties when they interact with electromagnetic radiations. This makes the absorption cross-section of these nanomaterials stronger than the strongest absorption molecules and the scattered light becomes intense than fluorescence of the organic dyes. The concept and ideas to fabricate nanoscale materials derived from chemistry, physics and engineering are integrated to design novel materials with desired properties. Nanomaterials involve the tailoring of materials at atomic level to attain unique properties, which can be suitably manipulated for the desired application.[12]

3.2. Hydrogels and their applications

Hydrogels have attracted considerable interest in the scientific research media because of its unique properties and variable applications. Hydrogels are novel materials

which have promising applications in various technological fields like biomedical, tissue engineering, pharmaceutical and other environmental technologies. The simplest definition of hydrogel states that the term hydrogel is a three-dimensional network structure of hydrophilic polymeric material. It possesses the ability to absorb large amount of water or water based fluids, swollen and retain the solution to form a hydrated interlinked penetrating network. The swelling capacity of hydrogel depends on the type of polymer backbone, extent of cross-linking and monomeric composition. In order a hydrogel to be conductive, its polymeric structure must combine the hydrogel structure with superior water absorption properties and includes doping with a conducting material like metals, metal oxides, conducting polymers etc.[13] The characteristics of such conducting hydrogels depend on both the concentration and structure of the metal oxides and polymers that is incorporated into the hydrogel matrix.

In this work, we synthesized the hydrogel of guar gum which is a polysaccharide made up of galactose and mannose. It is biodegradable, non-toxic, renewable raw material and low cost. Guar gum can be defined as a high-molecular weight, water soluble, non-ionic biopolymer extracted from endosperm of guar beans, which have been widely used in biomedical applications due to the change in its rheological properties. Here, we synthesize an aminated guar gum from guar gum by some chemical reaction that involves the ethylene diamine and sodium borohydride. The reaction includes the substitution of –OH group with $–NH_2$ group at the 2^{nd}, 3^{rd} and 6^{th} position in the monosaccharide unit of polysaccharide backbones of the polymer. This $–NH_2$ group plays a significant for immobilization of antibody as there is a covalent bond formation between the $–NH_2$ group of GGH and –COOH group of the antibody that leads to the formation of amide bond between them.[14] Therefore, GG has a good film forming ability, large surface area, biocompability and fascinating electron transfer ability. Exploiting the properties of ZrO_2 and GGH, the (ZrO_2-GGH) hybrid nanocomposites based electrode having thermal, electrical and tunable mechanical properties can be prepared with a low production cost that can be further used for the construction of a biosensor.[15]

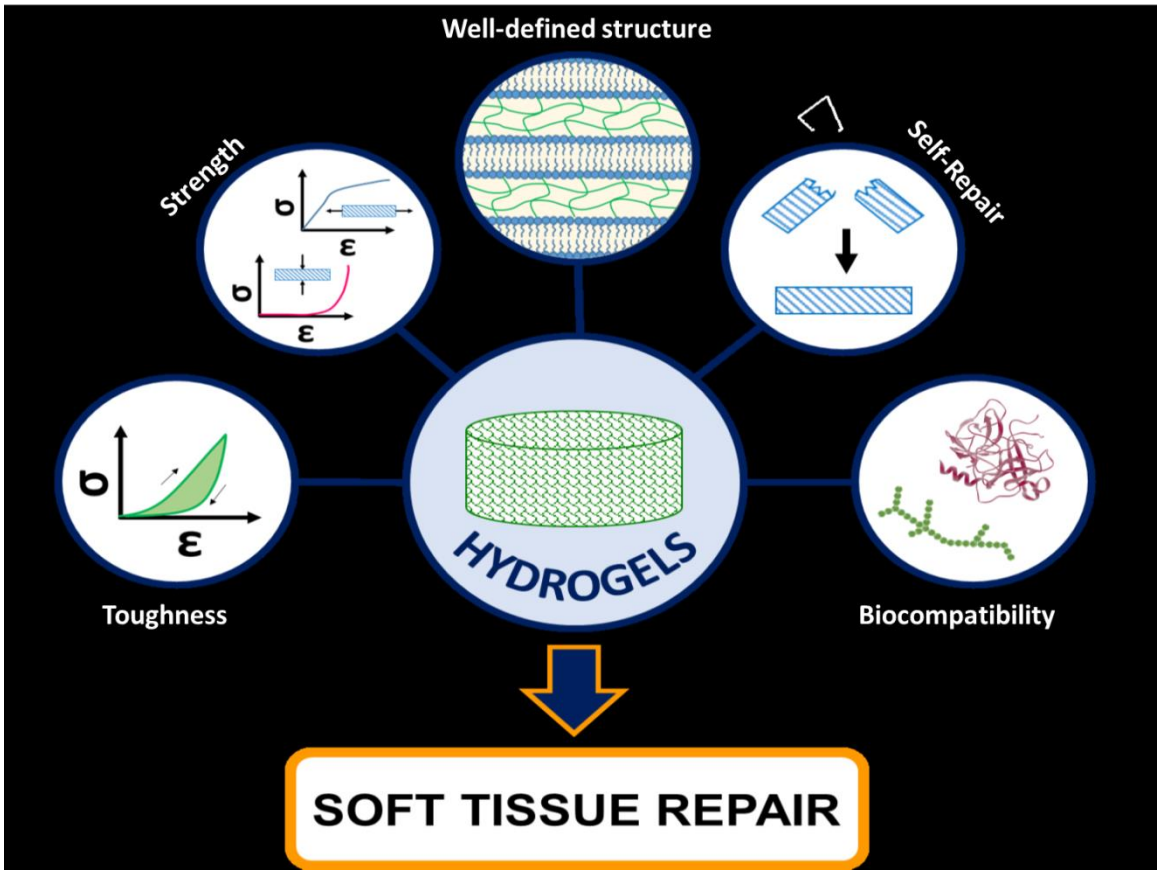

Figure 3.1: Graphical representation of basic characteristics of the hydrogel.

The nanocomposites composed of nanoparticles dispersed in GGH have attracted increased attention in the recent years and many researchers so called it hydrogel-nanoparticles nanocomposite. These hydrogel nanocomposites find wider range of applications in technical fields like catalysts, photographic materials, artificial muscles, memory devices and biosensor.

3.3. Biosensor

According to International Union of Pure and Applied Chemistry (IUPAC), biosensor is a self-contained integrated analytical device as it is capable of providing specific semi-quantitative or quantitative analytical information using a biological recognition element. It is used to detect the physio-chemical changes produced by specific interaction between the target analyte and biorecognition element which is detected by a transducer.[16] Biorecognition elements may be antibody, nucleic acid, whole cell or tissue, nucleic acid, receptor protein, enzyme. In the past decade, biosensors

have aroused increasing interest in biomedical and environmental monitoring due to their unique properties like high specificity, portability, speed, sensitivity and low cost.[17]

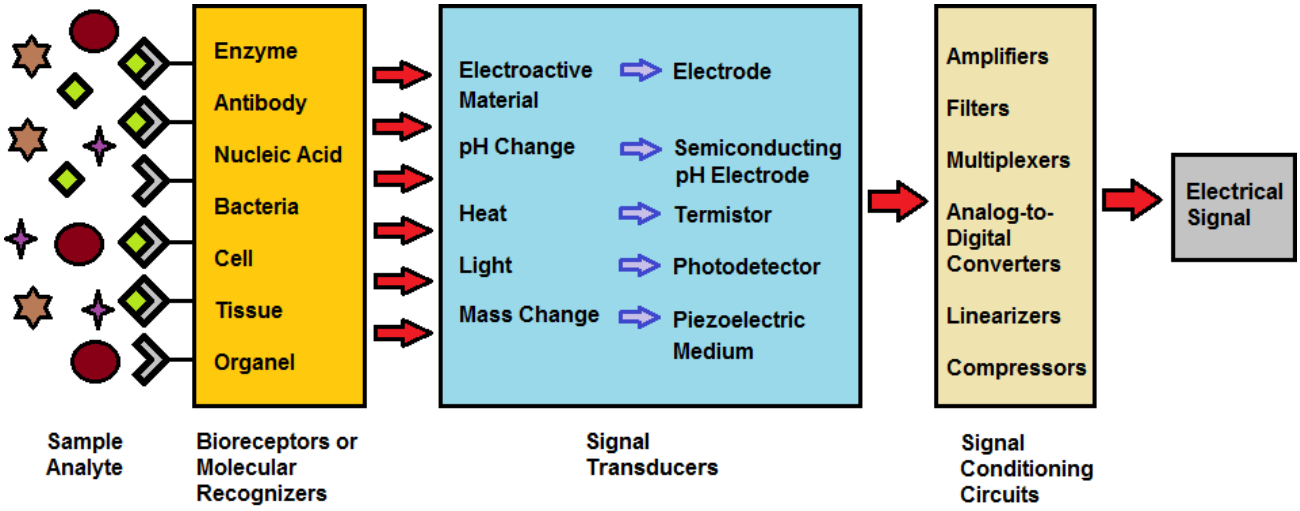

Figure 3.2: The basic structure and function of a biosensor.

3.3.1. Components of a biosensor

Biosensor can be classified into three major components: (a) a biological recognition element such as antibody, DNA, enzyme etc. for the recognition of analyte known as bio-receptor, (b) an immobilization matrix such as nanomaterials, sol-gel films, self-assembled monolayers and conducting polymers that are used for the immobilization of a biomolecule and (c) a transducer unit for conversion of biochemical reaction product into a recognizable signal. Bioreceptor alongwith transducer is also known as biosensor membrane.

3.3.1.1. Biomolecular recognition element

Biomolecular recognition element i.e. bioreceptor is a biological molecule that has the capability of recognizing a substrate i.e. an analyte. The most commonly used bioreceptors in biosensors are antibody, enzymes, nucleic acid or whole cells. These biomolecular recognition elements should have the ability to recognize biomarkers that are secreted in body fluids such as saliva, urine, sweat, blood etc. Among all these, the most prominent fluid is blood which is commonly used for the detection of biomarkers. The usage of blood sample in biomarkers recognition is invasive, high cost processing

and require clinical expert for sample collection, storage, handling etc. that makes the overall process highly complex. To minimize these limitations saliva could be a promising candidate for the detection or analysis of biomarkers.[18]

3.3.1.2. Immobilization matrix

An important part of a biosensor is a matrix which is used for the immobilization or integration of desired biological molecules at the surface of transducer. Besides this, matrix should effectively maintain the functionality of the biomolecules and at the same time provides receptivity towards the target analyte and acquainted with the transducer surface. The immobilization method for analyte and operational stability of a biosensor depends upon the chemical properties of immobilizing matrix. The characteristics of a favorable immobilizing matrix it should be resistant to a wide range of physiological temperature, ionic strength, pH and chemical composition.[19]

Among the different types of immobilizing matrices, nanostructured metal oxides achieved a great deal of attention due to their exceptional electronic and optical properties such as high mechanical and thermal stability, larger surface area, biocompatibility, abundant functional groups, and the ability towards the direct electron transfer of proteins or enzymes makes them ideal for the fabrication of a biosensor.[20-21]

3.3.1.3. Transducer

A transducer is a device which converts a biological signal received from biochemical activity between a biological component and an analyte into an electronic signal. Transducer can be classified into different types depending upon the type of signal received such as optical, electrochemical, thermal or piezoelectric transducer. Among them electrochemical transducer aroused much interest due to the simplicity, high signal-to-noise ratio, fast response time and high sensitivity. It offers many advantages over other transducers based biosensor, including lower detection range, high sensitivity, wide linear detection range, good stability, need lower sample amount etc.[22-23]

3.4 Cancer

Cancer is an uncontrolled division of cells with the potential to invade or spread to other parts of the body. Over 100 types of cancer that affects human. Tumors can be

classified into two types: begnin and malignant.[24] Not all the tumors are cancerous like begnin tumors do not spread to other parts of the body while malignant tumors spread to other to parts of the body via blood, body fluids etc. The possible symptoms of cancer include lump formation, prolonged cough, abnormal bleeding, loss of weight and change in bowel movements. The factors behind the cause of cancer chewing tobacco, alcohol consumption, poor diet, lack of physical activity, obesity, smoking, exposure to ionizing radiation, hepatitis viruses B and C, human papilloma virus (HPV) and environmental pollutants. These factors cause changes in genes of a cell that are required before the development of cancer.[25] Sometimes cancer is caused due to inherited genetic defects in person's parents. The use of tobacco causes of about 20% of cancer deaths. In 2012 about 14.1 million new cases of cancer deaths globally. [26]

3.5. Oral Cancer

All malignancies originating in oral or mouth cavity are known as oral cancer (OC). OC appears as uncontrolled growth or sore in the mouth cavity that does not heal. OC includes cancer of the lips, cheeks, tongue, floor of the mouth, hard and soft plate, sinuses and pharynx (throat).[15, 27] Squamous cell carcinoma, which develops in the tissue that line the mouth and lips or in lining of oral mucosa independently accounts for over 90% of OC. [28]

OC most commonly develops in older and middle aged individuals, but in recent years a large number of younger adults found with these malignancies. OC can be divided in to three categories on the basis of epidemiological and clinicopathological perspective: carcinomas of oral cavity, carcinomas of oropharynx and carcinomas of lips. Oropharyngeal malignancies are more common among male than female, with ratio of over 2:1. In contrast to oropharyngeal malignancies, carcinomas of the lips are more epidemiologically similar to squamous cell carcinomas of the skin and found primarily in men. These malignancies are strongly associated with chronic sun exposure although these carcinomas sometimes related to the specific site of the lips where cigarettes or other means of tobacco smoking habitually held.

The strong association between tobacco use and OC is well established. The risk of developing OC is 5-9 times greater for smokers in comparison to non-smokers, and this risk may increase to as much as 17 times greater for extremely heavy smokers of 80 or more cigarettes per day.[29] Approximately 80% of the OC patients are the smokers

which is two to three times greater than general OC (non smoker) patients. In addition, treated oral cancer patients who continue to smoke have a two to six time greater risk of developing a second malignancy of the upper aerodigestive tract than those who stop smoking. The use of Marijuana is also considered to be a potential risk factor responsible for the developing OC in younger adults.[30]

Snuff and chewing tobacco have also been associated with an increased risk for oral cancer. In addition, a significant number of oral cancers in smokeless tobacco users develop at the site of tobacco placement. However, the use of smokeless tobacco appears to be associated with a much lower cancer risk than that associated with smoked tobacco. Alcohol consumption has been identified as a major risk factor for OC. In studies controlled for smoking, moderate-to-heavy drinkers have been shown to have a 3-9 times greater risk of developing OC.[31] Patients who are both heavy smokers and heavy drinkers can have over one hundred times greater risk for developing a malignancy. In India and Southeast Asia, the chronic use of betel quid (*paan*) in the mouth has been strongly associated with an increased risk for oral cancer. Near about 75% of OC linked to tobacco and excessive alcohol consumption. Other factors include poor nutrition, poor oral hygiene and some chronic infection caused by bacteria and viruses.[28]

Recent studies suggest that some strains of human papillomavirus (HPV) may be associated with some oral and oropharyngeal cancers. HPV-16 and HPV-18 has been detected in up to 22 % and 14 % respectively of OC cases. Anaemia, iron deficiency in combination with dysphagia and esophageal webs (Plummer Vinson or Paterson-Kelly syndrome) is associated with an elevated risk for development of OC. Immunosuppression appears to predispose some individuals to an increased risk for oral cancer. Carcinomas of the lip have been reported in a number of kidney transplant patients receiving immunosuppressive medications, and oral carcinomas have been documented in young AIDS patients.[32]

Symptoms of OC include red, white and/or a mixture of these colors in patches, a non-healing sore on the face, neck and mouth or lips, pain and tenderness in any area of mouth, unexplained bleeding in mouth, loose teeth, chewing and swallowing difficulties, and change in voice.[33]

In order to increase the early detection of oral cancers, and by so doing increase the survival rates of oral cancer patients, there is therefore the need to identify diagnostic screening modalities that identify early oral malignant lesions with precision.

3.6. Conventional methods for detection of Oral Cancer

In recent years, number of techniques has been identified to improve the diagnosis and prognosis throughout the body but there is not the similar improvement in diagnosis and prognosis. Because 5 years survival in oral cancer patients is related to the stage at which cancer is diagnose, prevent and early efforts have the chances not only decreases the occurrence, but also improving the survival of those who develop this disease. Many conventional techniques include biopsy, visualization adjuncts, laser capture microdissection and cytopathology. There are also a number of methods that may contribute to the detection of OC.[34-36] Some of these are described below:

- **Light based detection methods:** Laser based diagnosis has been recently developed for the earlier detection of OC. These methods are mainly used to examine the mouth cavity as it helps to visualize lesions. It is mainly based upon the difference in absorbance of the abnormal metabolite and structural changes in cells.
- **Biopsy:** In this method, bristled catheter is used to collect the cells sample from the suspected area of OC. It is an invasive technique that is used to diagnose OC. The main drawback of this technique has been associated with brush biopsy is the only means of visualization the OC is poorly identified.
- **Cytological techniques:** The study of phenotypes and cellular functions of tissues or cells have been done by the different methods of molecular and cell biology. They all come under the cytological techniques.
- **Laser Capture Microdissection (LCM):** LCM is the technique which boosted the study of cancerous cells on molecular level by providing precise information. It is used to isolated carcinomas from the microscopic regions of tissues or cells with preserved cell morphology. Moreover, with the combination of histochemical staining, we can get more accurate information of cancerous cells. For better molecular diagnostic results, we can use SELDITOF-MS technology with LCM and bioinformatics.
- **Vital Staining:** Toluidine blue has been widely used for staining of cancerous cells. In this method, 1% of aqueous solution of TB has been applied over the lesion for 30 seconds. After that, acidophilic metachromatic nature of TB helps to differentiate between cancerous and normal cells. This staining method has been

found to be highly sensitive method to diagnose OC. The major drawback of this technique is about 58% it produce false negative results.

- **Microscopy:** The study of biochemical reaction of cells helps to detection the alteration in cell before the symptoms gets appeared morphologically. Spectral cytopathology (SCP) allow the collection of spectrum from an individual cell and detect internal biochemical changes arise due to disease. SCP works on principles of vibrational spectroscopy for detection of intracellular biochemical changes.

CHAPTER 4

MATERIALS AND METHODS

4. Materials and methods:

4.1. Chemicals and Reagents: Guar gum powder was procured from chemical drug house pvt. Ltd. Sodium borohydride ($NaBH_4$) and Ethylene diamine ($C_2H_8N_2$) were from Sigma-Aldrich Chemicals.1-(3-(dimethylamino)-propyl)-3-ethylcarbodiimide hydrochloride (EDC) [$C_8H_{17}N_3$] of AR grade were purchased from Sigma-Aldrich. Sodium hydroxide (NaOH) pellets, sodium monophosphate [NaH2PO4], sodium diphosphatedihydrate [$Na_2HPO_4{\cdot}2H_2O$], *N*-hydroxysuccinimide (NHS) [$C_4H_5NO_3$], sodium chloride [NaCl], potassium ferricyanide {$K_3[Fe(CN)_6]$}, and potassium ferrocyanide {$K_4[Fe(CN)_6]3H_2O$} were procured from Fisher Scientific. The amino acid Serine was also purchased from Sigma-Aldrich Chemicals. All chemicals were of analytical grade and were used without any further purification. Phosphate buffered saline (PBS) solution of pH 7.0 was prepared using $Na_2HPO_4{\cdot}2H_2O$ (0.05 mol L −1) and NaH_2PO_4 (0.05 mol L−1). Fresh PBS solution was prepared using Milli-Q water having resistivity of 18 MΩ cm and stored at 4 °C. The CYFRA-21-1 and anti-CYFRA-21-1 were obtained from Ray Biotech, Inc., India. These biomolecules were further diluted by using PBS buffer of pH 7.0. CYFRA-21-1 ELISA Kit was purchased from KinesisDX, USA. ELISA plate reader was from iMark, Bio red, USA.

4.2. Experimental

4.2.1. Synthesis of Hydrogel: The synthesis of hydrogel was carried out by the addition of ethylene diamine as an aminating agent to the guar gum, which substitutes the -OH group of the guar gum with $-NHCH_2CH_2NH_2$. Further, the $-NHCH_2CH_2NH_2$ has been reduced to $-NH_2$ group by the addition of $NaBH_4$. 1 gram of guar gum was dissolved in 250 mL of distilled water and continuously stirred to get homogeneous solution. Then, 25 mL of ethylene diamine was added to the homogeneous solution of guar gum and allowed to react with continuous stirring at room temperature for overnight. Then 50 mL of $NaBH_4$ solution was added to the reaction mixture was precipitated and washed several times with acetone. The powdered nanoparticles have been obtained.

4.2.2. Synthesis and functionalization of zirconia nanoparticles: Zirconium oxide nanoparticles have been synthesized by hydrothermal method. First of all, we prepared the separate solution of 0.2M zirconium ethoxide, 0.8M sodium hydroxide, 0.1M of CTAB were prepared in deionized water. The aqueous solution of CTAB was

dropped into the solution of zirconium ethoxide with constant stirring at 60℃ for 2hr. Subsequently, the solution of sodium ethoxide was added with continuous stirring for additional 2h. Then, there is a formation of homogenous solution which has been transferred into the Teflon vessel and placed in a stainless steel tank. After that, the Teflon vessel filled with homogenous solution was placed in an oven at 170℃ for 15 hr for hydrothermal reaction. After the reaction is completed, hydrothermal reactor was allowed to cool to the room temperature (25℃). The precipitate was obtained which has been washed with deionized water through the centrifugation process till the pH of the solution becomes neutral. Therefore, the slurry was dried at 100℃ overnight and annealed at 400℃ for 3h. Then, the mortar-pestle has been used to crush the product into fine powder for further characterization.

100 mg of ZrO_2 was added to 25 mL of isopropanol and kept it on sonication to obtain a highly dispersed solution. After that, 20 mg of Serine was added with continuous stirring for 48 hrs at room temperature (25℃). Next, add 10 mL of ddH_2O. Subsequently, suspension was dried in hot air oven at 100℃ for 7 hrs. Then, the sample obtained in powdered form.

4.2.3. Fabrication of biosensing platform: First of all, the solution of hydrogel was mixed with serine functionalized nanostructured zirconium oxide in 1:1 ratio followed with continuous stirring till the solution becomes viscous. The obtained viscous solution shows that functionalized nanoparticles get incorporated in the interpenetrating network of the hydrogel. After that, solution has been drop cast onto the prehydrolyzed ITO glass electrode then kept it in the oven for 30mins at the temperature of 60℃ for drying.

4.2.4. Collection of saliva sample of oral cancer patients: The saliva samples of oral cancer have been obtained from Rajiv Gandhi Cancer Institute and Research Centre, Delhi (India). An approved protocol was followed to collect the saliva samples provided by Rajiv Gandhi Cancer Institute and Research Center Institutional Review Board and all patients provided written consent. Samples were collected, processed and stored under similar conditions. The unstimulated whole saliva was collected from six patients

diagnosed for oral cancer. First of all, the mouth was rinsed with deionized water (5 mL) then the saliva was expectorated into sterilized tube, kept in ice condition. The collected saliva sample was centrifuged at 2800 rcf at room temperature for 30 min after which the supernatant was collected in a sterilized tube and stored at -20℃ until further used.

4.2.5. Quantification of CYFRA-21-1 present in saliva of oral cancer

Enzyme linked immunosorbent assay test (ELISA) was used for the quantification of CYFRA-21-1 in saliva samples of six oral cancer patients. Double sandwich ELISA technique was used in which anti-CYFRA-21-1 precoated microtiter 96 wells plat were used. Both the standard and patient's samples were used in triplicate. After implementation of all the steps, colorimetric reaction occurred and the absorbance was recorded at 450 nm in ELISA plate reader. A series of CYFRA-21-1 concentration in saliva samples has been used to validate the electrochemical response of the fabricated biosensor. It can be seen that a reasonable correlation exists between the magnitude of CV current response of the fabricated immunoelectrode in the presence of (a) CYFRA-21-1 concentrations in saliva samples determined by ELISA and (b) standard concentration of CYFRA-21-1. The results obtained exhibit acceptable %RSD (relative standard deviation) indicating high accuracy of the fabricated biosensor.[37]

4.3. Characterization

Crystallinity and phase information of synthesized product was obtained by using monochromatic X-ray diffraction (XRD) pattern [Bruker D-8 Advance] with Cu-Ka radiation (λ=1.5406 Å). Morphological observations and particle size were carried out using transmission electron microscopy at an accelerating voltage of 200 kV (Tecnai G2 30 U-twin, Tecnai 300 kV ultratwin microscope). The morphology of Guar gum, Hydrogel, $nZrO_2$ and Serine/$nZrO_2$/Hydrogel electrodes was investigated using XRD. Next, functional groups and bonds present in Serine, Serine functionalized zirconia nanoparticles (Serine/$nZrO_2$), Hydrogel and Serine/$nZrO_2$/Hydrogel were investigated through Fourier transform infrared spectroscopy (FT-IR) [PerkinElmer, Spectrum BX II]. The Autolab Potentiostat (Netherlands) was used for the electrochemical response studies by using a three-electrode system. The fabricated electrode acted as the working electrode, Ag/AgCl as the reference electrode and platinum (Pt) as the counter electrode.

4.3.1. X-ray Diffraction (XRD) Technique

Max von Laue, in 1912, discovered that crystalline substances act as three-dimensional diffraction gratings for X-ray wavelengths similar to the spacing of planes in a crystal lattice. X-ray diffraction is an effective tool in studying the nature of crystalline substances. It is based on constructive interference of monochromatic X-rays and a crystalline sample. These X-rays are generated by a cathode ray tube, filtered to produce monochromatic radiation, collimated to concentrate, and directed toward the sample. The interaction of the incident rays with the sample produces constructive interference (and a diffracted ray) when conditions satisfy Bragg's Law (**Eq. 4.1**)

$$2d \, Sin \, \theta = n \, \lambda \quad \ldots\ldots\ldots\ldots \quad \textbf{Eq. 4.1}$$

where λ is the wavelength of electromagnetic radiation, θ is the diffraction angle and d is the lattice spacing in a crystalline sample. These diffracted X-rays are then detected, processed and counted. By scanning the sample through a range of 2θ angles, all possible diffraction directions of the lattice is attained due to the random orientation of the powdered material. This technique is used to characterize the crystallographic structure, crystallite size (grain size) and preferred orientation in polycrystalline or powder solid samples.

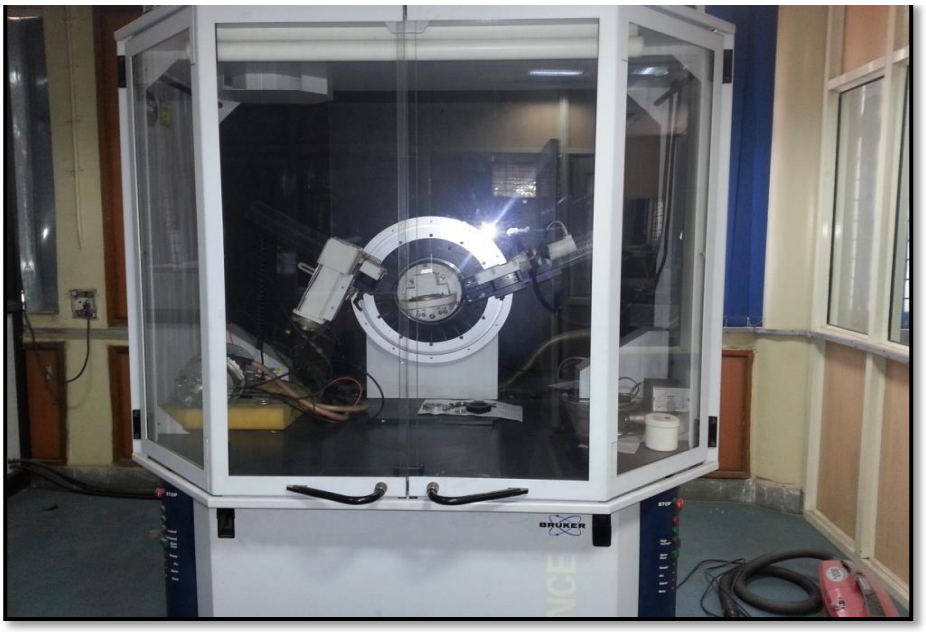

Figure 4.1: X-Ray Diffraction (XRD) Instrument.

XRD can be applied to characterize the heterogeneous solid mixture to determine relative abundance of a crystalline compound. It is also useful in providing information on the structure of unknown sample when coupled with lattice refinement technique such as relative refinement. XRD patterns are recorded on X-ray diffractometer, wherein the peak broadening data are obtained by measuring the average of peak broadening in the five strongest diffraction peaks. The mean size of the nanoparticles is determined from the peak broadening in the X-ray diffraction pattern by using **Debye– Scherrer equation (Eq. 2)**.

$$\boldsymbol{D = \frac{0.9\lambda}{\beta Cos\theta}} \text{..... Eq. 4.2}$$

where D is the average crystallite size (Å), λ is wavelength of X-rays (Cu Kα: λ = 1.5418 Å), θ is the Bragg diffraction angle, and β is the full width at half maximum (FWHM) (in radians). The sample under study can be of either a thin layer of crystal or in powder form. Since, the power of a diffracted beam is dependent on quantity of corresponding crystalline substance; it is also possible to carry out quantitative determinations using this technique.

Precautions:

i) The film should be considerably thick to eliminate the substrate interference.

ii) To perform the powder XRD, there should be adequate quantity of sample so that the perfect diffraction is achieved.

4.3.2. Scanning electron microscopy (SEM)

Electron Microscopes are scientific instruments that use a beam of highly energetic electrons to examine objects on a very fine scale. This examination can yield information about the topography (surface features of an object), morphology (shape and size of the particles making up the object), composition (the elements and compounds that the object is composed of and the relative amounts of them) and crystallographic information (how the atoms are arranged in the object) [208]. Electron Microscopes (EMs) are similar in operation to optical microscopes except that they use a focused beam of electrons instead of light to "image" the specimen.

Figure 4.2: Scanning electron microscope (SEM) Instrument.

Figure 4.2 shows the Schematic revealing the components of scanning electron microscope. Here a beam of electrons is produced at the top of the microscope by an electron gun. Normally tungsten is used in thermionic electron guns owing to its highest melting point and lowest vapor pressure of all metals; however lanthanum hexabromide can also be used if the vacuum system is upgraded. The electron beam is confined and focused using metal apertures and magnetic lenses into a thin, focused, monochromatic beam. This beam is focused onto the sample using a magnetic lens. The electron beam is

scanned over the specimen in a series of lines and frames called a raster. Once the beam hits the sample, electrons and X-rays are ejected from the sample. Detectors collect these X-rays, backscattered electrons and secondary electrons and convert them into a signal that is sent to a screen similar to a television screen producing final image. An attachment called Energy dispersive X-ray spectroscopy is also used in SEM for the elemental analysis of the specimen. Here, X-ray spectrometer converts X-ray photon into an electrical pulse which is measured by a multi-channel analyzer. The analyzer records increments in corresponding "energy slot" and shows on a monitor display. The location of the slot is proportional to energy of the X-ray photon entering the detector. The display is a histogram of the X-ray energy received by the detector, with individual peaks, the heights of which are proportional to the amount of a particular element in the specimen being analyzed.

Precautions:

i) If the sample conductance is poor then a few Å thick conductive gold coating should be done by sputtering before analysis in order to have better resolution.

ii) The dimension of the sample should be ~ 0.5 cm × 0.5 cm.

4.3.3. Electrochemical Techniques

Electrochemical techniques relate the changes of an electrical signal to an electrochemical reaction at an electrode surface, usually as a result of an imposed potential or current. In a solution, the equilibrium concentrations of the reduced and oxidized forms of a redox couple are linked to the potential (E) via the Nernst's Equation (Eq. 4.3).

$$E = E_o + \frac{RT}{nF} + \ln \frac{C_{oxi}}{C_{red}} \quad \text{..... Eq. 4.3}$$

where, E_O is equilibrium potential, F is Faraday's constant, T is absolute temperature, C_{oxi} and C_{red} are concentrations of oxidation and reduction centers. If the potential E is applied to the working electrode with respect to the reference electrode e.g. via Potentiostat, the redox couples present at the electrode respond to this change and adjust their concentration ratios according to Eq. 4.3.

Figure 4.3. Autolab Potentiostat/Galvanostat, EcoChemie, Netherland.

DPV is one of the most widely used pulse techniques in electrochemistry. Electrochemical pulse methods involve the modulation of potential in order to increase speed and sensitivity of measurement. DPV consists of a series of potential pulses of fixed amplitude (10-100 mV) superimposed on to a slowly changing base potential. The time interval of each potential step in this series is ~40-50 ms. The current is measured at two time points of the pulse – first, just before the pulse starts and second when the pulse ends. The difference between the current values at these two points (δi) is plotted against the base potential. The resulting plot of δi vs. V is referred to as a differential pulse voltammogram consisting of current peak(s), the height of which is directly proportional to the concentration of the corresponding analyte(s). The relationship between the peak current and concentration of analyte is given by the expression –

$$\mathbf{I_p} = \frac{nFAD^{1/2}C}{\sqrt{\pi t_m}} \frac{(1-\sigma)}{(1+\sigma)} \quad \textbf{..... (4.4)}$$

where n is the no. of electrons involved, F is Faraday's constant, A is electroactive surface area, D is diffusion coefficient, C is the concentration of the electroactive species, t_m is the time after pulse when current is sampled, and $\sigma = \exp[(nF/RT)(\Delta E/2)]$ (ΔE is the pulse amplitude). For large values of ΔE, the maximum value of $(1-\sigma)/(1+\sigma)$ is unity.

The value of charging current is mathematically described by the following equation –

$$I_c \approx -0.00567 C C_i \Delta E m^{2/3} t^{-1/3} \ldots\ldots\ldots\ldots \textbf{(4.5)}$$

where C_i is the integral capacitance. It is clear from the above equation that the 'differential-pulse' operation leads to a fast decay of charging current. This decreases the contribution of charging current to the faradaic current leading to accurate results. In other words, DPV offers an added advantage of lower charging current and allows measurements at concentrations as low as 10^{-8} M (Wang, J, 2006). Any unknown analyte involved in the redox reaction can be determined by the peak potential (E_p) as it is related to the half-wave potential by the following equation –

$$\mathbf{E_p = E_{1/2} - \Delta E/2 \ldots\ldots\ldots\ldots (4.6)}$$

The peak width at half-height can be used to determine the number of electrons involved in the reaction by the following equation –

$$W_{1/2} = \frac{3.52RT}{nF} \ldots\ldots\ldots\ldots \textbf{(4.7)}$$

Thus, a one-electron stoichiometry corresponds to a peak width of 30.1 mV at room temperature (Wang, J., 2006).

CHAPTER 5

RESULTS AND DISCUSSION

5. Results and Discussion:

5.1. Structural and morphological studies

Figure shows the pattern of Guar Gum, Hydrogel, Serine/nZrO_2 and Serine/nZrO_2/Hydrogel which were characterized through XRD technique in the range of 2θ angle from 20˚ to 70˚. The XRD pattern of guar gum shows number of different peaks at 22˚, 32˚, 39˚, 45˚, 55˚ and 67˚ that show the polysaccharide structure of guar gum. Figure (b) shows the peaks mainly at 22˚, 30˚, 32˚, 35˚ and 40˚ represents the formation of polymeric network of the hydrogel.[3, 38] Five peaks are indexed at 24.2˚, 28.3˚, 31.7˚, 34.7˚ and 45.7˚ indicating the formation of the monoclinic phase of zirconia molecules in the planes of (110), (111), (-111), (200) and (-211), respectively (JCPDS No. 37-1484). There are few peaks seen at 30.3˚, 50.5˚ and 60.2˚ indicate presence of tetragonal phase of ZrO_2 in the planes of (101), (112) and (211), respectively (JCPDS No. 80-2155). These two different monoclinic and tetragonal phases reveal the formation of mixed phase of zirconia nanoparticles.

The average crystallite size "D" the nanoparticles has been estimated to be ~4.5 nm by using Debye-Scherrer equation as given below-

$$\boldsymbol{D = \frac{0.9\lambda}{\beta Cos\theta}} \quad \text{..... (5.1)}$$

where λ = 1.540 Å is the wavelength of the target Cu-Kα, θ is the Bragg's diffraction angle, and β is the full width at half maximum (FWHM) of the diffraction peak.

The figure (d) shows peaks of both zirconia nanoparticles and hydrogel i.e. 24˚, 28˚, 31.5˚, 35˚, 50˚, 55˚ and 60˚ reveal the incorporation of serine functionalized zirconia nanoparticles into the interpenetrating network (IPN) of hydrogel.

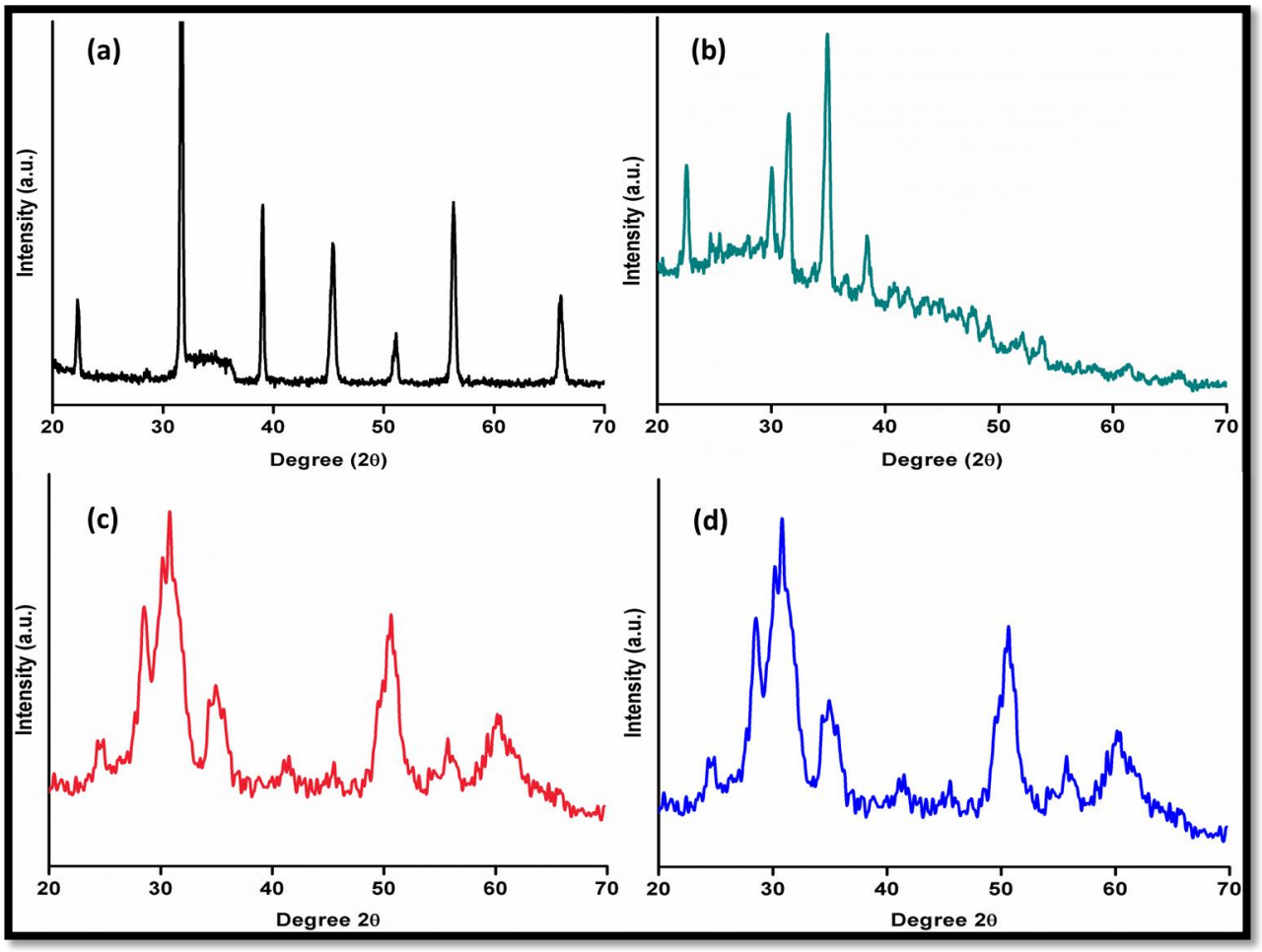

Figure 5.1: XRD of (a) Guar gum, (b) Hydrogel, (c) $nZrO_2$ and (d) Serine/$nZrO_2$/Hydrogel.

5.2. Scanning Electron Microscopy studies

The SEM was used to analyze the surface morphology of guar gum, hydrogel, nanoparticles incorporated hydrogel and antibody immobilized hydrogel. SEM images clearly shows the pure guar is solid sheet like structure while the surface topography of hydrogel can be analyzed through the SEM; however, the synthesized hydrogel limits the effectiveness of this analytical method as SEM can only be used on samples with low water content, hydrogel must be dried before observation, and the resulting artefacts alter the surface morphology. Despite this, hydrogel shows interpenetrating network (IPN). However, hydrogel in its hydrated state can provide more useful information on the material characteristics expected for the implant material. Figure (c) shows that the white colored particles are nanostructured serine functionalized zirconia which incorporated into the network of the hydrogel. Figure (d) shows antibody has been immobilized onto the serine functionalized nanoparticle.

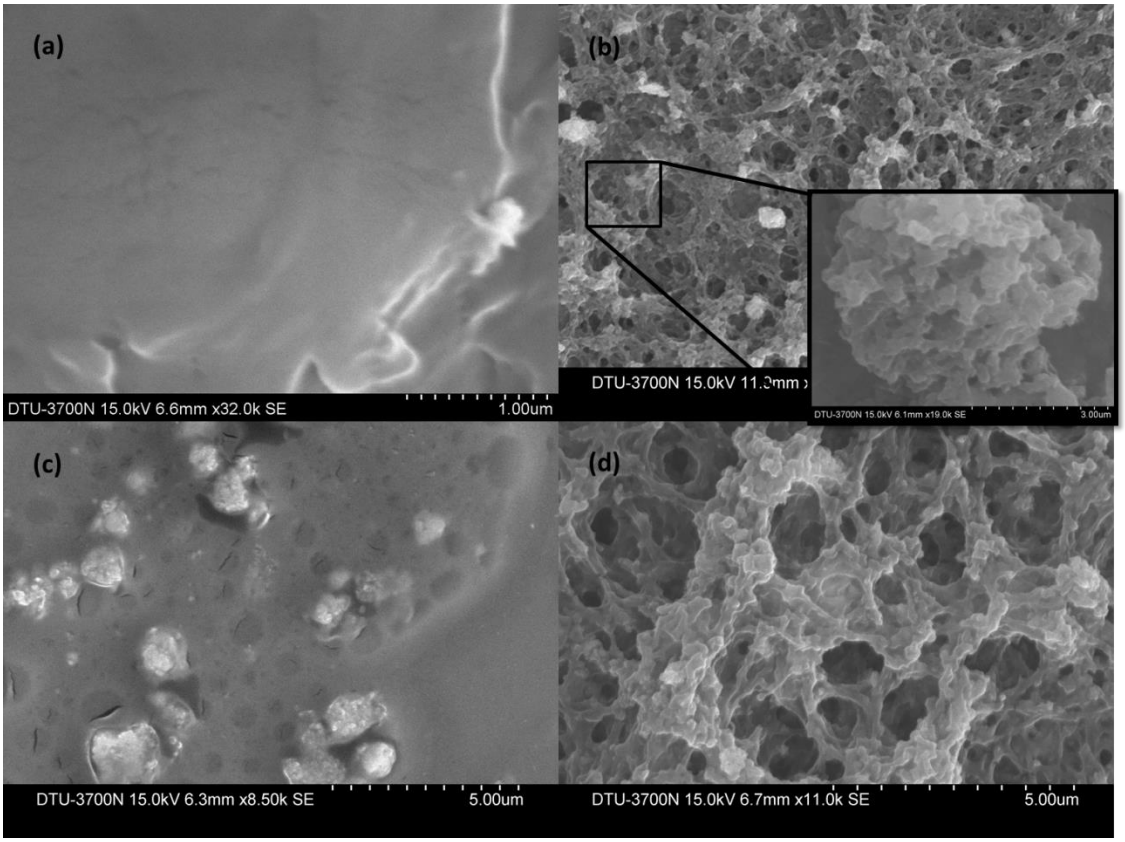

Figure 5.2: SEM images of (a) Guar Gum, (b) Hydrogel, (c) Serine/nZrO$_2$/Hydrogel and (d) anti-CYFRA-21-1/Serine/nZrO$_2$/Hydrogel/ITO.

5.3.Electrochemical studies

5.3.1. Electrode studies

The differential pulse voltammetry (DPV) studies on ITO, Serine/nZrO$_2$/ITO, Serine/nZrO$_2$/Hydrogel/ITO, anti-CYFA-21-1/Serine/nZrO$_2$/Hydrogel/ITO and BSA/anti-CYFRA-21-1/Serine/nZrO$_2$/Hydrogel/ITO electrodes respectively in PBS solutions (50 mM, pH 7.0, 0.9% NaCl) containing 5 mM of $[Fe(CN)_6]^{3-/4-}$ at a scan rate of 10 mV s^{-1} in the potential range, -0.4 to 0.6V. It was found that the magnitude of peak current obtained for Serine/nZrO$_2$/ITO electrode is 0.17 mA and in case of the Serine/nZrO$_2$/Hydrogel/ITO electrode is 0.28 mA. This is attributed to the excellent physiological properties of hydrogel which imply the continuous release of nanoparticles from the interpenetrating network of hydrogel into the external environment.[39] After immobilization of the antibodies i.e. anti-CYFRA-21-1/Serine/nZrO$_2$/Hydrogel/ITO immunoelectrode shows increase in peak current i.e. 0.32 mA, which may be due to presence of Serine/nZrO$_2$/Hydrogel nanocomposite matrix that acts as a mediator at the

electrode surface (ITO) resulting in significant increase of the electron tunneling distance between the antibodies and the electrode.[40-42] Therefore, the electrostatic interaction between the free site of the antibodies (-NH_2 terminal) and redox species may results in fast electron diffusion towards the immunoelectrode. After the immobilization of BSA, there is decrease in the magnitude of peak current i.e. 0.26 mA due to non-specific adsorption of BSA onto the exposed Serine/$nZrO_2$ sites of the anti-CYFRA-21-1/Serine/$nZrO_2$/Hydrogel/ITO immunoelectrode.[43]

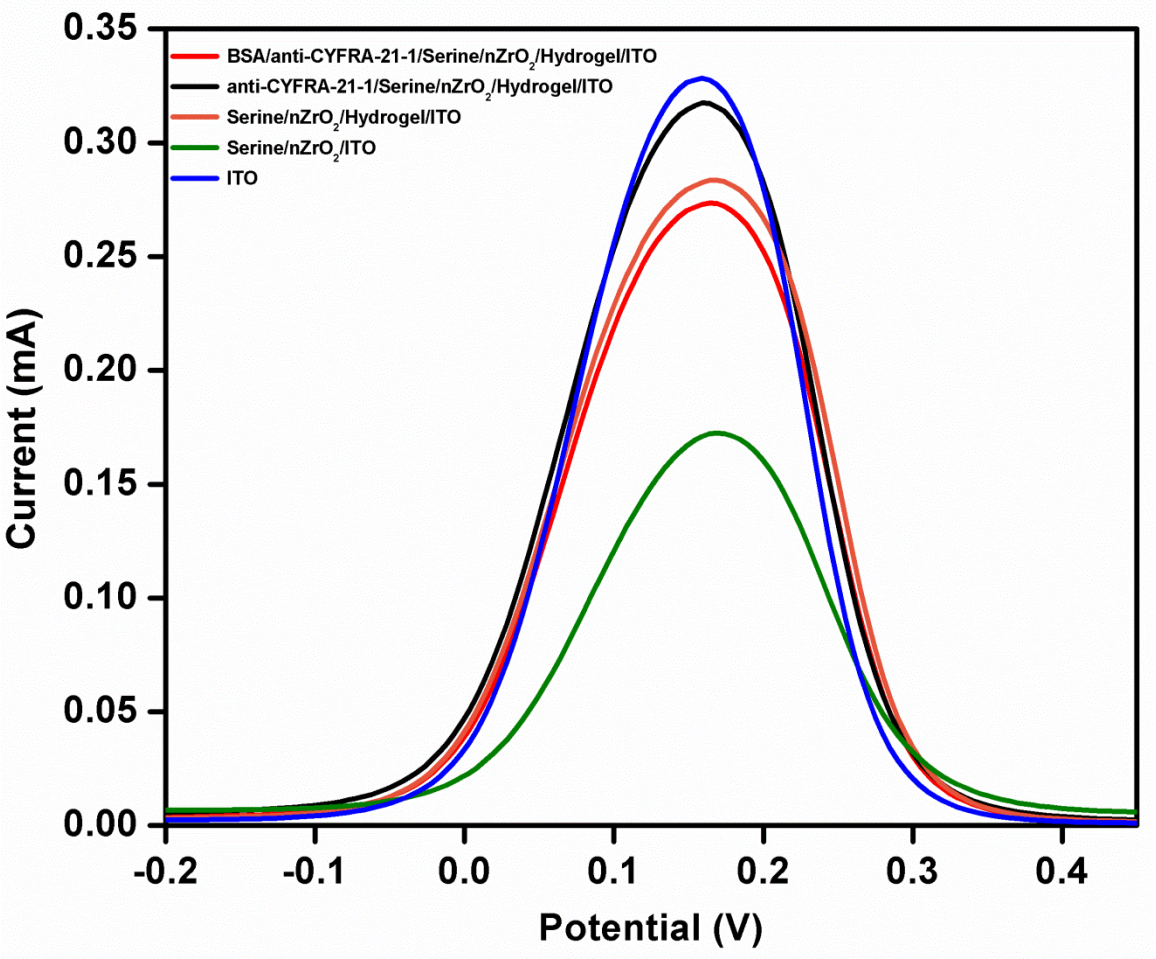

Figure 5.3: Differential pulse voltammetry (DPV) of BSA/anti-CYFRA-21-1/Serine/$nZrO_2$/Hydrogel/ITO, anti-CYFRA-21-1/Serine/$nZrO_2$/Hydrogel/ITO, Serine/ $nZrO_2$/Hydrogel/ITO, Serine/$nZrO_2$/ITO and ITO electrodes.

Further, for studying the electron transfer capability of Serine/$nZrO_2$/Hydrogel/ITO and Serine/$nZrO_2$/ITO electrochemical impedance spectroscopy (EIS) was performed in the frequency range 100 KHz to 0.1 Hz at a biasing potential of 10 mV using 0.05 M PBS

containing 5×10^{-3} M $[Fe(CN)_6]^{3-/4-}$ ions. The HET rate (K˚) was calculated using the following equation.

$$\mathbf{Rct = RT/F^2k^{\circ}C \ldots\ldots\ldots\ldots\ldots (5.2)}$$

where, R is molar gas constant, T is the temperature, F is the Faraday constant and C is the concentration of the electroactive species, Rct is the charge transfer resistance which is a characteristic of the electrode surface. The HET of the Serine/$nZrO_2$/Hydrogel/ITO electrode is (6.073×10^{-7}) and Serine/$nZrO_2$/ITO electrode is (2.252×10^{-7}) indicating HET value of Serine/$nZrO_2$/Hydrogel/ITO electrode is approximately 4 times fold higher than that of Serine/$nZrO_2$/ITO electrode.

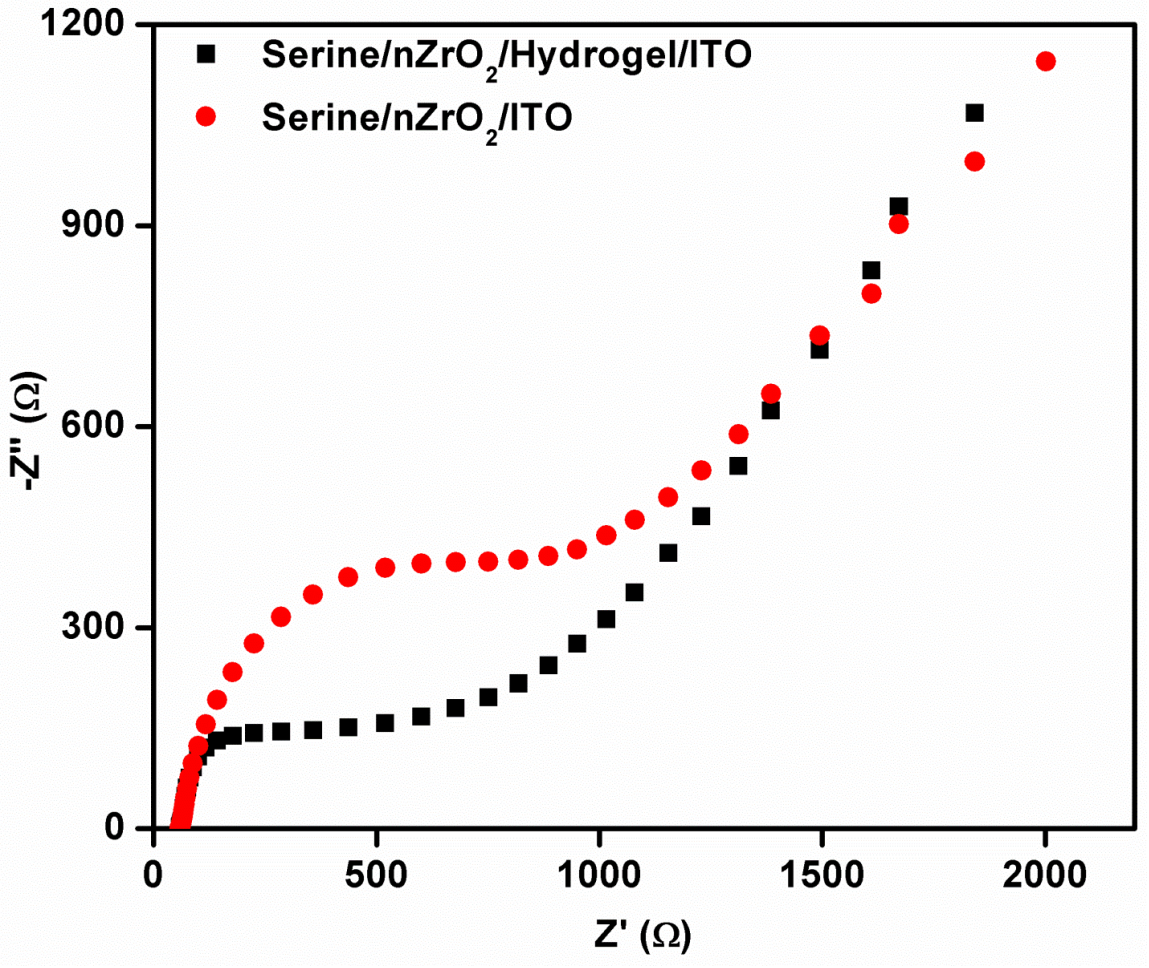

Figure 5.4: Electrochemical impedance spectroscopy (EIS) of Serine/nZO_2/Hydrogel/ITO and Serine/$nZrO_2$/ITO.

5.3.2. pH studies

By using differential pulse voltammetry (DPV) technique, the electrochemical response of the BSA/anti-CYFRA-21-1/Serine/nZrO_2/Hydrogel/ITO immunoelectrode as a function of pH (6.0 to 8.0) was investigated at the scan rate of 50 mV s^{-1} in phosphate buffer saline (PBS) containing 5×10^{-3} M $[Fe(CN)_6]^{3-/4-}$. It can be seen that the maximum peak current at neutral pH 7.0.[44] This may perhaps be due to the fact that biological molecules such as amino acids, antigen, antibody, enzymes etc. are present in natural form at with high specific activity at neutral pH. Therefore, in acidic or basic medium antibodies get denatured due to the interaction H^+ or OH^- ion on amino acid sequence of antibodies. Thus, PBS buffer with pH 7.0 was used for all the electrochemical studies.

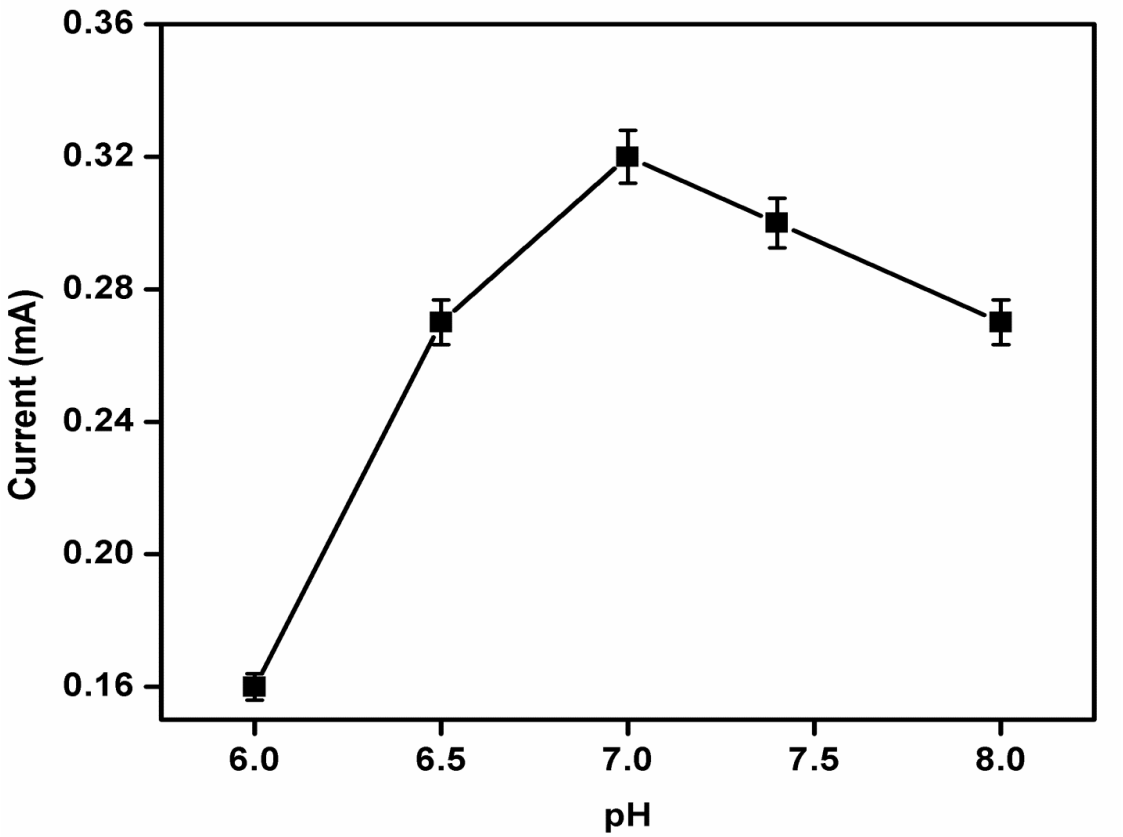

Figure 5.5: Current response of the BSA/anti-CYFRA-21-1/Serine/nZrO_2/Hydrogel/ITO immunoelectrode as a function of pH.

5.3.3. Scan rate studies

The cyclic voltammetry (CV) response of Serine/nZrO_2/Hydrogel/ITO and BSA/anti-CYFRA-21-1/Serine/nZrO_2/Hydrogel/ITO electrodes was shown as a function

of scan rate (40-190 mV s^{-1}), respectively. We observed that the magnitude of both cathodic (I_{pc}) and anodic (I_{pa}) peak current exhibit a linear relationship with the square root of scan rate, indicating the electrochemical reaction is a diffusion-controlled process.

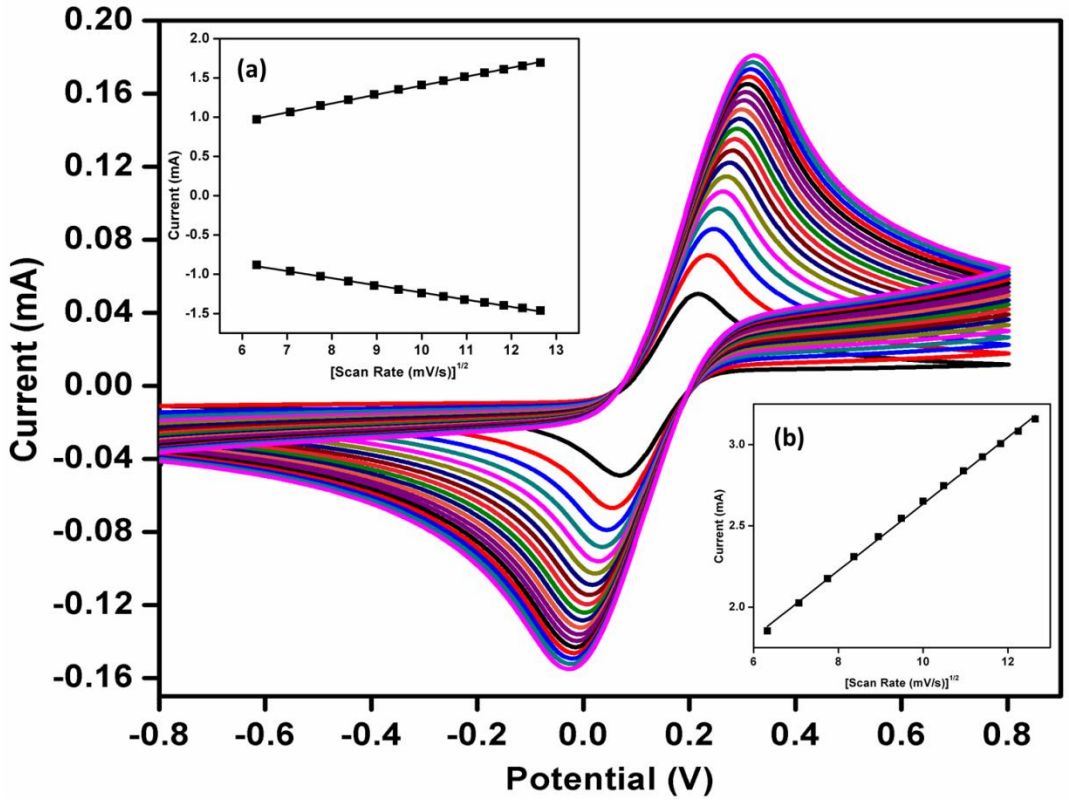

Figure 5.6: Cyclic voltammetry (CV) of BSA/anti-CYFRA-21-1/Serine/nZrO_2/Hydrogel/ITO electrode as a function of scan rate (40-190 mV/s). Magnitude of oxidation and reduction current response as a function of scan rate (mV/s) (inset a), and difference of cathodic and anodic peak potential (ΔEp) as a function of scan rate (inset b).

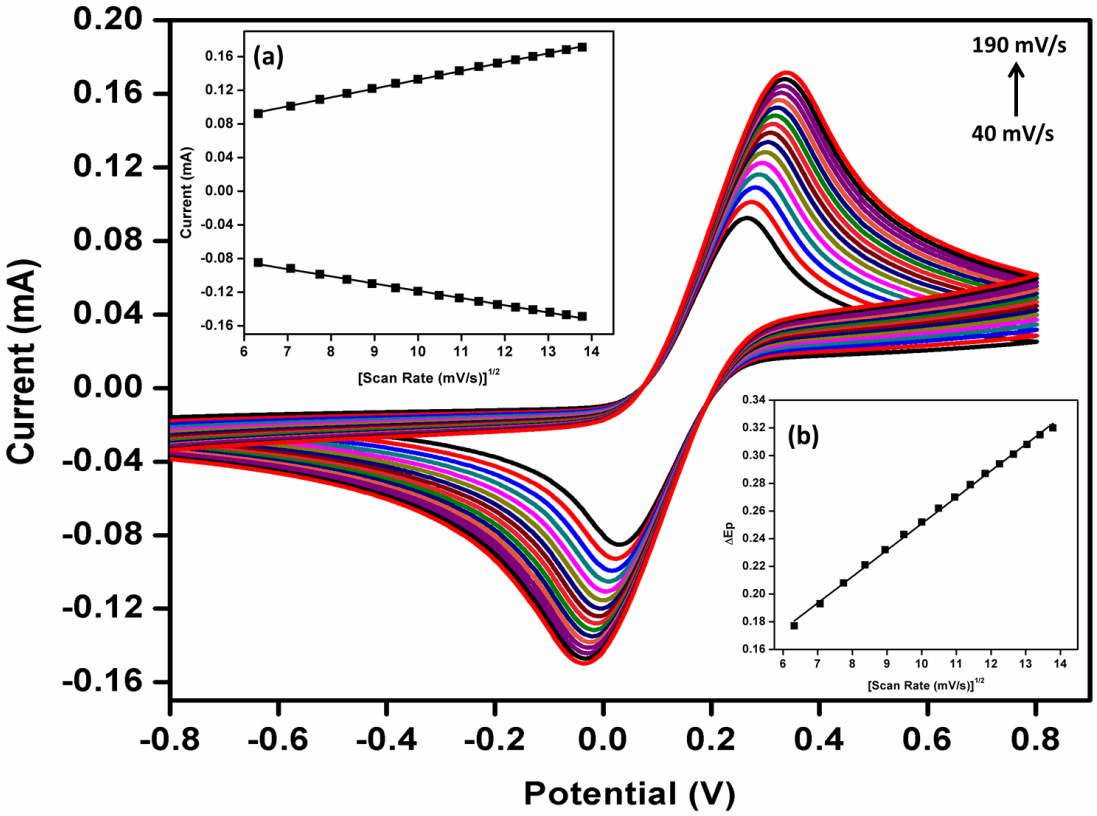

Figure 5.7: Cyclic voltammetry (CV) of Serine/nZrO_2/Hydrogel/ITO electrode as a function of scan rate (40-190 mV/s). Magnitude of oxidation and reduction current response as a function of scan rate (mV/s) (inset a), and difference of cathodic and anodic peak potential (ΔEp) as a function of scan rate (inset b).

The slopes and intercepts are given by the equations below-

$I_{pa(Serine/nZrO2/Hydrogel/ITO)}$ = [0.11 mA(sm V^{-1}) × (scan rate [mV s^{-1}])$^{1/2}$] + 0.27 mA, R^2 = 0.99,

SD = 9.53×10^{-3} …… (5.3)

$I_{pc(Serine/nZrO2/Hydrogel/ITO)}$ = -[0.08 mA(sm V^{-1}) × (scan rate [mV s^{-1}])$^{1/2}$] – 0.32 mA, R^2 = 0.99, SD = 1.23×10^{-2} …… (5.4)

$I_{pa(BSA/anti-CYFRA-21-1/Serine/nZrO2/Hydrogel/ITO)}$ = [0.11 mA(sm V^{-1}) × (scan rate [mV s^{-1}])$^{1/2}$] + 0.26 mA, R^2 = 0.99, SD = 9.78×10^{-3} …….(5.5)

$I_{pc(BSA/anti-CYFRA-21-1/Serine/nZrO2/Hydrogel/ITO)}$ = [0.09 mA(sm V^{-1}) × (scan rate [mV s^{-1}])$^{1/2}$] – 0.32 mA, R^2 = 0.99, SD = 1.21×10^{-2} …….. (5.6)

After which it was observed that with increasing scan rate, the oxidation peak current shifts towards the higher potential and the reduction peak shifts towards lower potential. The linearity has been obtained between the difference in magnitude of the oxidation peak potential and reduction peak potential ($\Delta V = V_{pa} - V_{pc,}$ where V_{pa} is anodic peak potential and V_{pc} is cathodic peak potential) as a function of scan rate, indicating amiable charge transfer kinectics between medium to electrode and follows Eqs. (6) and (7):

$\Delta E_p(V)_{Serine/nZrO2/Hydrogel/ITO}$ = [0.2 V (smV^{-1}) × (scan rate [mVs^{-1}])$^{1/2}$] + 0.58 V, R^2 = 0.99, SD = 2.18×10^{-2}……. (5.7)

$\Delta E_p(V)_{BSA/anti-CYFRA-21-1/Serine/nZrO2/Hydrogel/ITO}$ = [0.19 V(smV^{-1}) × (scan rate [mVs^{-1}])$^{1/2}$] + 0.59 V, R^2 = 0.99, SD = 2.13×10^{-2}…… (5.8)

Where R is the correlation coefficient and SD is the standard deviation.

5.3. Incubation time studies

The above figure shows the variation of current obtained via CV on interaction of CYFRA-21-1 with the BSA/anti-CYFRA-21-1/Serine/$nZrO_2$/Hydrogel/ITO immunoelectrode for different incubation times. We observe an increase in current with respect to incubation time from 2 to 35 min. However, after 28 min of sample incubation the current becomes nearly constant. Thus, we have selected the sample incubation time as 28 min during which the antigen–antibody binding reaction reaches the steady state.

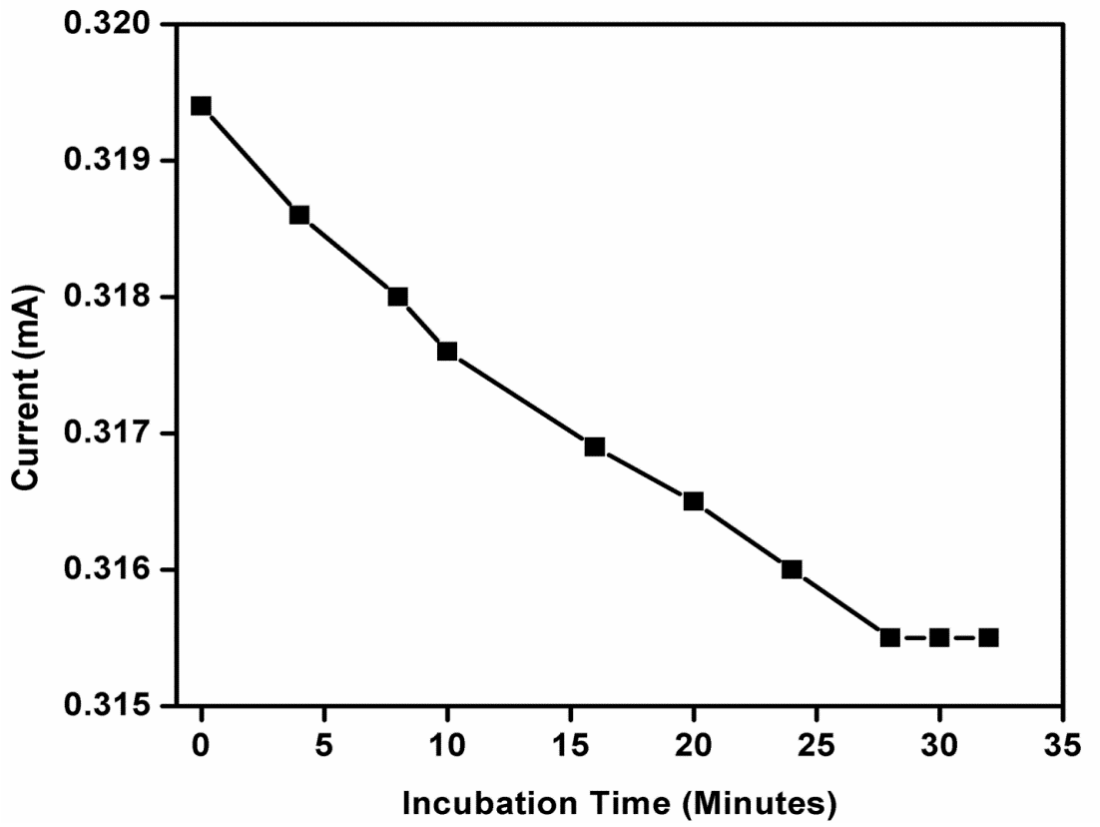

Figure 5.8: Incubation time studies for binding of CYFRA-21-1 with BSA/anti-CYFRA-21-1/Serine/nZrO_2/Hydrogel/ITO immunoelectrode.

5.4. Electrochemical response studies

The Differential Pulse Voltammetry (DPV) technique has been used to investigate the electrochemical behavior of the fabricated immunoelectrode BSA/anti-CYFRA-21-1/Serine/nZrO_2/Hydrogel/ITO as a function of CYFRA-21-1 concentration in PBS buffer (50 mM, 0.9% NaCl) containing $[Fe(CN)_6]^{3-/4-}$ (5 mM). All the measurements have been repeated three times for each concentration. It has been found that there is an decrease in the magnitude of anodic peak current after the formation of antigen-antibody complex between CYFRA-21-1 and anti-CYFRA-21-1 on the electrode.[45]

Under optimized assay conditions, the curve between different concentration of CYFRA-21-1 and BSA/anti-CYFRA-21-1/Serine/nZrO_2/Hydrogel/ITO immunoelectrode shows linear range in the concentration of 2.5 to 80 ng mL^{-1} after which the current tends to saturate at higher concentrations with a linear regression coefficient of 0.993. The sensitivity of the fabricated immunoelectrode can be estimated by the slope of the curve and is found to be 0.86 μA mg^{-1} mL cm^{-2}. The limit of detection and standard deviation

of the immunoelectrode are obtained to be 2.5 and 80 ng mL^{-1}. The limit of detection has been calculated using the standard equation.

Limit of detection = 3σ/sensitivity …… (5.9)

where σ is standard deviation of the BSA/anti-CYFRA-21-1/Serine/$nZrO_2$/Hydrogel/ITO immunoelectrode.

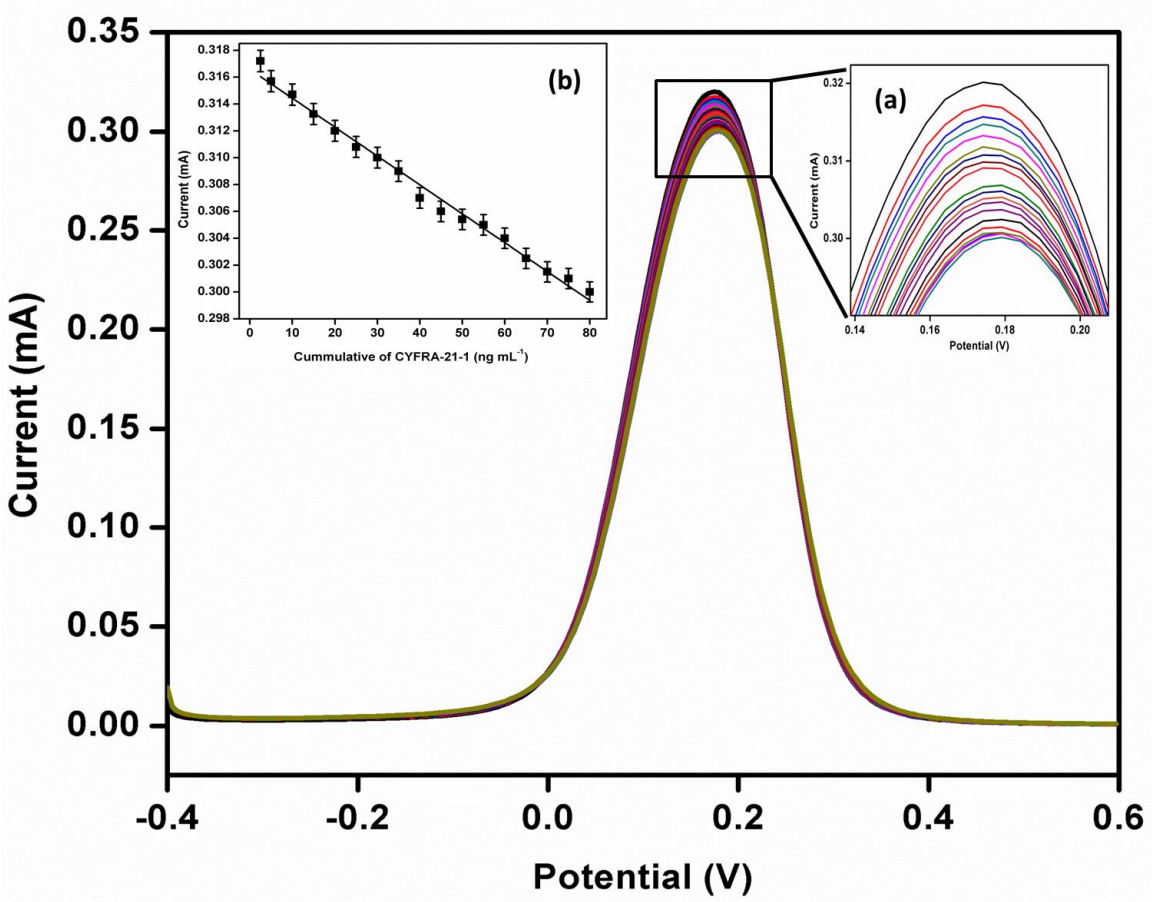

Figure 5.9: Electrochemical response of BSA/anti-CYFRA-21-1/Serine/$nZrO_2$/Hydrogel/ITO immunoelectrode as a function of CYFRA-21-1 concentration (2.5-80 ng mL^{-1}). The magnify view of oxidation peak current (inset (a)). Calibration curve between magnitude of peak current and concentration of CYFRA-21-1 (ng mL^{-1}) (inset (b)).

5.5. Control studies

The control experiment has been conducted to investigate the electrochemical response of Serine/$nZrO_2$/Hydrogel/ITO electrode as a function of CYFRA-21-1

concentration. There is no observable change in the current response of the Serine/$nZrO_2$/Hydrogel/ITO electrode with increasing concentration of CYFRA-21-1 antigen. It may be due to Serine/$nZrO_2$/Hydrogel/ITO electrode surface does not interact with antigen molecule and therefore the electrochemical change remains unchanged.

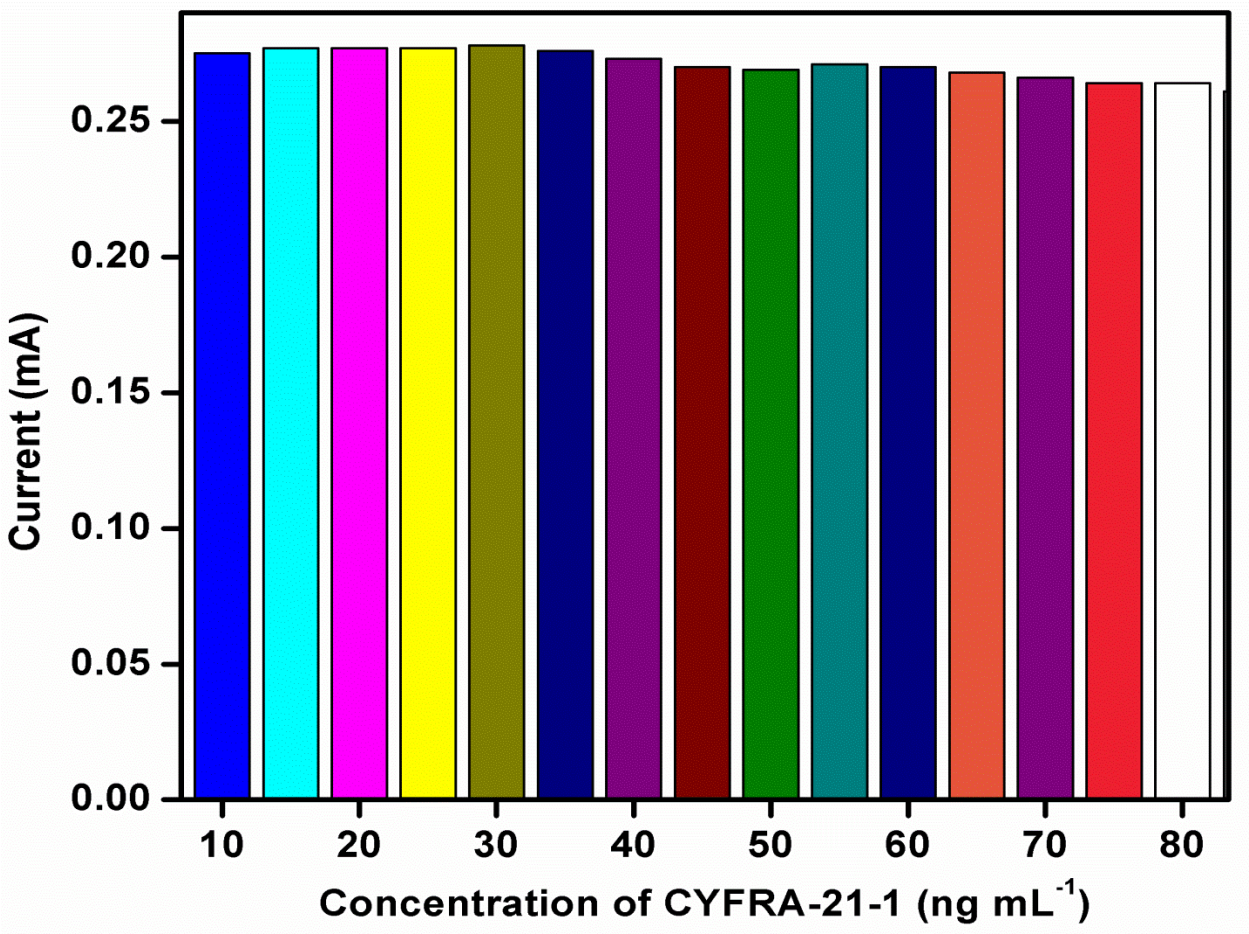

Figure 5.10: Control experiment (through electrochemical response study) of Serine/ $nZrO_2$/ITO electrode as a function of CYFRA-21-1 concentration (2.5-80 ng mL^{-1}).

5.6. Interferents and ions effect studies

As we know saliva get saturated with a large number of organic, inorganic and biological analytes such as Carcinoembryonic antigen (CEA) [4-16 ng mL^{-1}], Sodium carboxymethyl cellulose (NaCM) [10 mg mL^{-1}], cardiac troponin I (cTn^{-1}) [0.19 ng mL^{-1}], glucose [7 ng mL^{-1}], endothelin-1 protein [1 pg mL^{-1}], glucose [7 mg mL^{-1}], ascorbic acid [0.24 µg mL^{-1}], lactic acid [0.03 µg mL^{-1}], sodium citrate [5 µg mL^{-1}] etc. We observed the effect of these interferences that the magnitude of the oxidation current increases upon addition of CEA, cTn-1, glucose and NaCMC respectively which represent the high selectivity of the biosensor towards CYFRA-21-1.

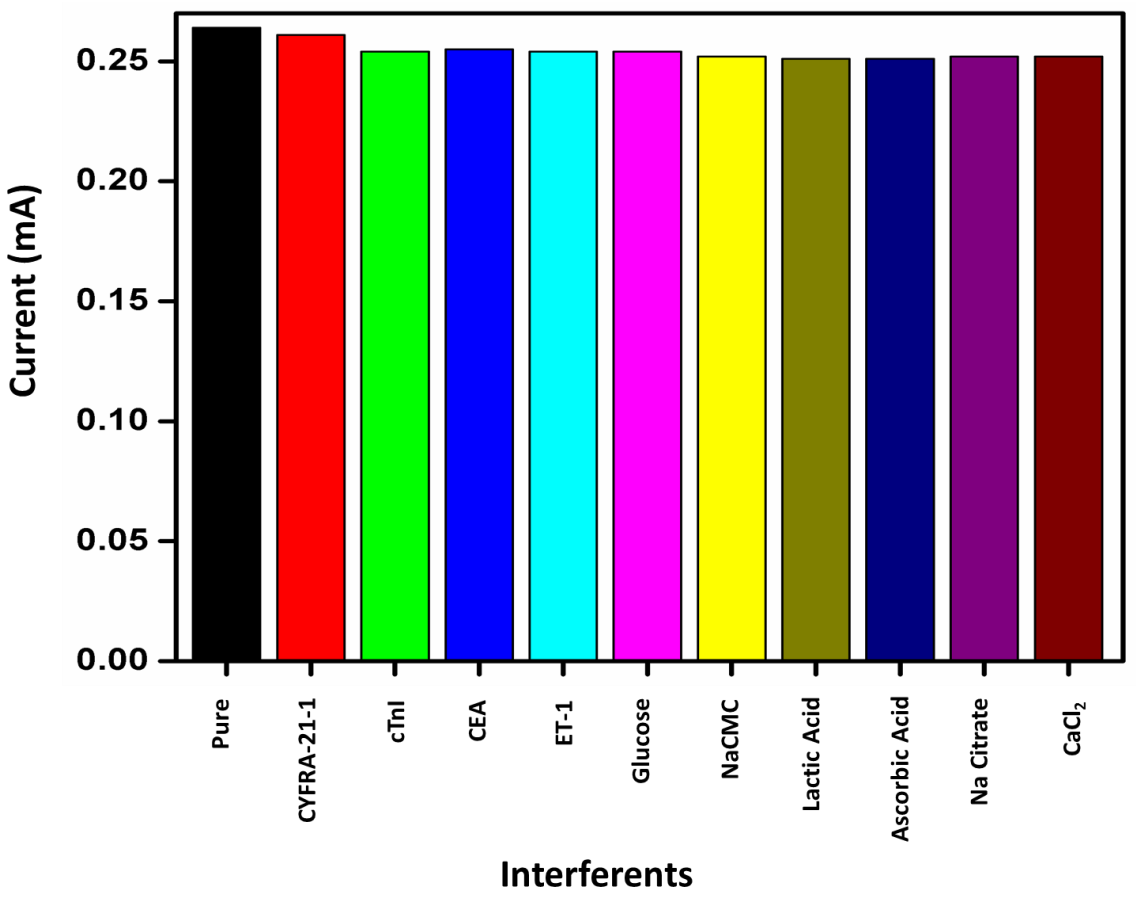

Figure 5.11: Interferent studies of BSA/anti-CYFRA-21-1/Serine/nZrO_2/Hydrogel/ITO immunoelectrode.

To investigate the effect of addition of analytes or ions as well as the effect of addition of different amount of artificial saliva samples which we prepared artificially. We have taken different quantities of artificial saliva were used against the immunoelectrode BSA/anti-CYFRA-21-1/Serine/nZrO_2/Hydrogel/ITO and observed the electrochemical response. It has been observed that the peak current response was stable upto addition of 1000 μL of artificial saliva after that it tends to decrease. This result represents that the peak current response upto 1000 μL does not influence by the presence of analytes as well as ions. We took 20 μL of each sample for the electrochemical response studies BSA/anti-CYFRA-21-1/Serine/nZrO_2/Hydrogel/ITO. The study was done under the same set of conditions with concentration of CYFRA-21-1 (0.01 ng mL^{-1}). We did not find any significant change in current that shows the immunoelectrodes exhibits high reproducibility.

5.7. Shelf life studies

The shelf life study of immunoelectrode BSA/anti-CYFRA-21-1/Serine/nZrO_2/Hydrogel/ITO has been predicted by measuring DPV at regular intervals in standard solution of CYFRA-21-1 in PBS at one week interval. It was observed that there is no significant change in electrochemical current upto 48 days after which decrease in the peak current was observed.

A manuscript containing results of the studies is currently under prepration and will be communicated to a suitable journal for publication shortly.

Table 2. Characteristics of the various detection techniques used for oral cancer detection.

Method	Detection Technique	Invasive/ Non-invasive	Label	Sample	Biomarker	Platform	Concentration range of biomarker	Linear detection range	Response time	Lower detection limit	Reference
Cytopathology	Staining	Invasive	-----	Cells	-----	-----	-----	-----	1 week	-----	[46]
Biopsy	Cell culture	Invasive	------	Tissue	------	-----	------	-----	2-3 weeks	-----	[47]
Visualization adjuncts	Staining	Invasive	------	Tissue	------	-----	------		1 week	-----	[47]
Biosensor	Amperometric	Invasive	Yes	Serum	IL-6 (Protein)	-----	≤6 pg mL^{-1} to ≥20 pg mL^{-1}	0.5-30 pg mL^{-1}	-----	-----	[48]
	DPV	Invasive	Yes	Serum	IL-6 (Protein)	-----	<6 pg mL^{-1} to >20 pg mL^{-1}	0.002-20 ng mL^{-1}	------	-----	[49]
	CV	Non Invasive	Yes	Saliva	has-miR-200a (mi-RNA)	-----	------	1aM-10fM	------	-----	[50]
	CV	Non Invasive	No	Saliva	CYFRA-21-1 (Protein)	BSA/anti-CYFRA-21-1/APTES/ ZrO_2/ITO	0-18 ng mL^{-1}	2-16 ng mL^{-1}	20 min	0.08 ng mA^{-1} mL^{-1}	[15]
	DPV	Non Invasive	No	Saliva	CYFRA-21-1 (Protein)	BSA/anti-CYFRA-21-1/APTES/ZrO_2-RGO/ITO	0-18 ng mL^{-1}	2-22 ng mL^{-1}	16 min	0.122 ng mA^{-1}	[27]
	DPV	Non Invasive	No	Saliva	CYFRA-21-1 (Protein)	BSA/anti-CYFRA-21-1/Serine/ ZrO_2/ITO	0-18 ng mL^{-1}	0.01-29 ng mL^{-1}	6 min	0.01 ng mA^{-1}	24
	DPV	Non Invasive	No	Saliva	CYFRA-21-1(Protein)	BSA/anto-CYFRA-21-1/Serine/nZrO2/ Hydrogel/ITO	0-18 ng mL^{-1}	2.5-80 ng mL^{-1}	24 min		Present Work

S = Sesitivity, LDR = Linear Detection Range, SL = Shelf life

CHAPTER 6

CONCLUSIONS

We have proposed a biocompatible hydrogel as an alternative for long term release of $nZrO_2$ nanoparticles which were functionalized with non-toxic amino acid i.e. Serine and having application in the fabrication of an efficient, label free and non-invasive biosensing platform for oral cancer biomarker (CYFRA-21-1) detection. First of all, we have synthesized hydrogel from a natural polysaccharide guar gum. Beside this, we synthesized nanostructured through one step low temperature hydrothermal process and further functionalized with serine molecules through simple chemical process. Serine functionalized zirconia (Serine/$nZrO_2$) was further incorporated into the presynthesized hydrogel in the 1:1 proportion. After that, the obtained viscous solution was drop cast onto the ITO glass electrode and dried at the temperature of 40℃. Further the obtained thin film of Serine/$nZrO_2$/Hydrogel/ITO was biofunctionalized with anti-CYFRA-21-1 with the help of EDC-NHS covalent surface chemistry and BSA was used to block the non-specific binding sites of immunoelectrode. The fabricated BSA/anti-CYFRA-21-1/Serine/$nZrO_2$/Hydrogel/ITO is simple and covers the whole physiological range of the secretion of CYFRA-21-1, secreted in human saliva samples with linear detection range 0.08 ng mL^{-1}, sensitivity 0.86 mA mg^{-1} mL ng^{-1} and stability upto 48 days. Fabrication of nanocomposite of hydrogel and nanostructured zirconia opens a new window in fabrication of biosensing platform as well as in drug delivery, tissue repair and in bioimaging systems.

CHAPTER 7

FUTURE PERSPECTS

The present experimental investigations reveal that the zirconia (MO_x) can efficiently be utilized in the development of high performance electrochemical biosensing devices with high sensitivity, selectivity, stability and design flexibility for both laboratory and point-of-care applications. There is enough scope to develop new approaches in making metal oxide materials. Further, these should be utilized in the real sample analysis for the detection of other potent disease biomarkers. Besides this, studies should be carried out to explore the application of these matrices for the development of toxin biosensors and other immunosensors.

Since the introduction of microfluidics technology in the early 1990s, an enormous amount of effort has been conducted towards the development of microfluidic immunosensors that combine the analytical power of microfluidic devices with the high specificity of antibody–antigen interactions. Recently, microfluidics technology coupled with nanoscience and nanotechnology are becoming powerful tools in biosensors fabrication, due to the advantages of high performance, design flexibility, reagent economy, high throughput, miniaturization, and automation. These miniaturized chip devices can notably change the speed and scale towards highly specific and selective antibody–antigen interactions. Attributing to the interesting physiochemical properties of the MO_xs, it would be interesting to incorporate MO_xs and there derivative in microfludic devices which would further open a new area of research and probably meet the real challenge in high performance biosensing. It is anticipated that the microfludic biosensors based on these MO_xs will soon lead to decisive improvements in quality of human life. Keeping above in view, it should be interesting to commercialize some of the MO_xs based biosensor for application in clinical diagnostics.

CHAPTER 8

REFERENCES

[1] M. Pandey, M.C.I. Mohd Amin, N. Ahmad, M.M. Abeer, Rapid synthesis of superabsorbent smart-swelling bacterial cellulose/acrylamide-based hydrogels for drug delivery, International Journal of Polymer Science, 2013(2013).
[2] P. Malik, M. Srivastava, R. Verma, M. Kumar, D. Kumar, J. Singh, Nanostructured SnO 2 encapsulated guar-gum hybrid nanocomposites for electrocatalytic determination of hydrazine, Materials Science and Engineering: C, 58(2016) 432-41.
[3] E. Abdel-Halim, S.S. Al-Deyab, Electrically conducting silver/guar gum/poly (acrylic acid) nanocomposite, International journal of biological macromolecules, 69(2014) 456-63.
[4] D. Zhai, B. Liu, Y. Shi, L. Pan, Y. Wang, W. Li, et al., Highly sensitive glucose sensor based on Pt nanoparticle/polyaniline hydrogel heterostructures, ACS nano, 7(2013) 3540-6.
[5] D. Pasqui, A. Atrei, G. Giani, M. De Cagna, R. Barbucci, Metal oxide nanoparticles as cross-linkers in polymeric hybrid hydrogels, Materials letters, 65(2011) 392-5.
[6] A.M. Costa, J.F. Mano, Extremely strong and tough hydrogels as prospective candidates for tissue repair–A review, European Polymer Journal, 72(2015) 344-64.
[7] Y. Lu, W. He, T. Cao, H. Guo, Y. Zhang, Q. Li, et al., Elastic, conductive, polymeric hydrogels and sponges, Scientific reports, 4(2014).
[8] R. Byakodi, S. Byakodi, S. Hiremath, J. Byakodi, S. Adaki, K. Marathe, et al., Oral cancer in India: an epidemiologic and clinical review, Journal of community health, 37(2012) 316-9.
[9] J. Chen, J. Zhang, Y. Guo, J. Li, F. Fu, H.-H. Yang, et al., An ultrasensitive electrochemical biosensor for detection of DNA species related to oral cancer based on nuclease-assisted target recycling and amplification of DNAzyme, Chemical Communications, 47(2011) 8004-6.
[10] W.V. Giannobile, T. Beikler, J.S. Kinney, C.A. Ramseier, T. Morelli, D.T. Wong, Saliva as a diagnostic tool for periodontal disease: current state and future directions, Periodontology 2000, 50(2009) 52-64.
[11] B.D. Fahlman, Nanomaterials, Materials Chemistry, Springer2011, pp. 457-583.
[12] P.R. Solanki, A. Kaushik, V.V. Agrawal, B.D. Malhotra, Nanostructured metal oxide-based biosensors, NPG Asia Materials, 3(2011) 17-24.
[13] R.M. Desai, S.T. Koshy, S.A. Hilderbrand, D.J. Mooney, N.S. Joshi, Versatile click alginate hydrogels crosslinked via tetrazine–norbornene chemistry, Biomaterials, 50(2015) 30-7.
[14] R. Murali, P. Vidhya, P. Thanikaivelan, Thermoresponsive magnetic nanoparticle–aminated guar gum hydrogel system for sustained release of doxorubicin hydrochloride, Carbohydrate polymers, 110(2014) 440-5.
[15] S. Kumar, S. Kumar, S. Tiwari, S. Srivastava, M. Srivastava, B.K. Yadav, et al., Biofunctionalized nanostructured zirconia for biomedical application: a smart approach for oral cancer detection, Advanced Science, 2(2015).
[16] D.R. Thévenot, K. Toth, R.A. Durst, G.S. Wilson, Electrochemical biosensors: recommended definitions and classification, Biosensors and Bioelectronics, 16(2001) 121-31.
[17] A. Koyun, E. Ahlatcolu, Y. Koca, S. Kara, Biosensors and their principles, A Roadmap of Biomedical Engineers and Milestones, (2012).

[18] M. Gerard, A. Chaubey, B. Malhotra, Application of conducting polymers to biosensors, Biosensors and Bioelectronics, 17(2002) 345-59.
[19] T. Ahuja, I.A. Mir, D. Kumar, Biomolecular immobilization on conducting polymers for biosensing applications, Biomaterials, 28(2007) 791-805.
[20] A.A. Ansari, A. Aldwayyan, M. Alhoshan, M. Alsalhi, Nanostructured metal oxides based enzymatic electrochemical biosensors: INTECH Open Access Publisher; 2010.
[21] A.A. Ansari, P.R. Solanki, A. Kaushik, B. Malhotra, Recent advances in nanostructured metal oxides based electrochemical biosensors for clinical diagnostics, Nova Science Publishers: Hauppauge, NY, USA2009.
[22] I. Sinclair, Sensors and transducers: Newnes; 2000.
[23] P.R. Solanki, A. Kaushik, P. Chavhan, S. Maheshwari, B. Malhotra, Nanostructured zirconium oxide based genosensor for Escherichia coli detection, Electrochemistry Communications, 11(2009) 2272-7.
[24] M. Macaluso, M.G. Paggi, A. Giordano, Genetic and epigenetic alterations as hallmarks of the intricate road to cancer, Oncogene, 22(2003) 6472-8.
[25] R.W. Clapp, G.K. Howe, M.M. Jacobs, Environmental and occupational causes of cancer: a call to act on what we know, Biomedicine & Pharmacotherapy, 61(2007) 631-9.
[26] M.J. Thun, J.O. DeLancey, M.M. Center, A. Jemal, E.M. Ward, The global burden of cancer: priorities for prevention, Carcinogenesis, 31(2010) 100-10.
[27] S. Kumar, J.G. Sharma, S. Maji, B.D. Malhotra, Nanostructured zirconia decorated reduced graphene oxide based efficient biosensing platform for non-invasive oral cancer detection, Biosensors and Bioelectronics, 78(2016) 497-504.
[28] S. Tiwari, P.R. Solanki, Emerging Aid in Oral Cancer Diagnosis, Journal of Molecular Biomarkers & Diagnosis, 6(2015) 1.
[29] N.K. Proia, G.M. Paszkiewicz, M.A.S. Nasca, G.E. Franke, J.L. Pauly, Smoking and smokeless tobacco-associated human buccal cell mutations and their association with oral cancer—a review, Cancer Epidemiology Biomarkers & Prevention, 15(2006) 1061-77.
[30] N. Firth, Marijuana use and oral cancer: a review, Oral oncology, 33(1997) 398-401.
[31] N.N. Ismail, K.I. Mokhtar, Absence of nucleotide alteration in region of exon 34 of NOTCH1 and NOTCH2 receptor genes analysed in oral cancer samples: a preliminary observation, Archives of Orofacial Sciences, 5(2010) 17-23.
[32] M.B. Kastan, J. Bartek, Cell-cycle checkpoints and cancer, Nature, 432(2004) 316-23.
[33] S. Kumar, S. Kumar, S. Tiwari, S. Augustine, S. Srivastava, B.K. Yadav, et al., Highly sensitive protein functionalized nanostructured hafnium oxide based biosensing platform for non-invasive oral cancer detection, Sensors and Actuators B: Chemical, 235(2016) 1-10.
[34] K. Masthan, N.A. Babu, K.C. Dash, M. Elumalai, Advanced diagnostic aids in oral cancer, Asian Pacific Journal of Cancer Prevention, 13(2012) 3573-6.
[35] S. Silverman, Oral cancer: PMPH-USA; 2003.
[36] C. Scully, J.V. Bagan, C. Hopper, J.B. Epstein, Oral cancer: current and future diagnostic techniques, Am J Dent, 21(2008) 199-209.
[37] E.T. Lee, J. Wang, Statistical methods for survival data analysis: John Wiley & Sons; 2003.
[38] A. Guiseppi-Elie, Electroconductive hydrogels: synthesis, characterization and biomedical applications, Biomaterials, 31(2010) 2701-16.

[39] R.A. Green, S. Baek, L.A. Poole-Warren, P.J. Martens, Conducting polymer-hydrogels for medical electrode applications, Science and Technology of Advanced Materials, (2016).
[40] J. Anusha, H.-J. Kim, A.T. Fleming, S.J. Das, K.-H. Yu, B.C. Kim, et al., Simple fabrication of ZnO/Pt/chitosan electrode for enzymatic glucose biosensor, Sensors and Actuators B: Chemical, 202(2014) 827-33.
[41] R.M. Pasternack, S. Rivillon Amy, Y.J. Chabal, Attachment of 3-(aminopropyl) triethoxysilane on silicon oxide surfaces: dependence on solution temperature, Langmuir, 24(2008) 12963-71.
[42] A. Vasudev, A. Kaushik, S. Bhansali, Electrochemical immunosensor for label free epidermal growth factor receptor (EGFR) detection, Biosensors and Bioelectronics, 39(2013) 300-5.
[43] M.A. Ali, C. Singh, K. Mondal, S. Srivastava, A. Sharma, B.D. Malhotra, Mesoporous Few-Layer Graphene Platform for Affinity Biosensing Application, ACS applied materials & interfaces, 8(2016) 7646-56.
[44] G. Liu, Y. Lin, Electrochemical sensor for organophosphate pesticides and nerve agents using zirconia nanoparticles as selective sorbents, Analytical chemistry, 77(2005) 5894-901.
[45] S. Srivastava, V. Kumar, M.A. Ali, P.R. Solanki, A. Srivastava, G. Sumana, et al., Electrophoretically deposited reduced graphene oxide platform for food toxin detection, Nanoscale, 5(2013) 3043-51.
[46] D. Rosenberg, S. Cretin, Use of meta-analysis to evaluate tolonium chloride in oral cancer screening, Oral Surgery, Oral Medicine, Oral Pathology, 67(1989) 621-7.
[47] L.L. Patton, J.B. Epstein, A.R. Kerr, Adjunctive techniques for oral cancer examination and lesion diagnosis: a systematic review of the literature, The Journal of the American Dental Association, 139(2008) 896-905.
[48] R. Malhotra, V. Patel, J.P. Vaqué, J.S. Gutkind, J.F. Rusling, Ultrasensitive electrochemical immunosensor for oral cancer biomarker IL-6 using carbon nanotube forest electrodes and multilabel amplification, Analytical chemistry, 82(2010) 3118-23.
[49] T. Li, M. Yang, Electrochemical sensor utilizing ferrocene loaded porous polyelectrolyte nanoparticles as label for the detection of protein biomarker IL-6, Sensors and Actuators B: Chemical, 158(2011) 361-5.
[50] J.-H. Wang, B. Wang, Q. Liu, Q. Li, H. Huang, L. Song, et al., Bimodal optical diagnostics of oral cancer based on Rose Bengal conjugated gold nanorod platform, Biomaterials, 34(2013) 4274-83.